The Landscape of the Hubbard model

Subir Sachdev

TASI lectures, June 2010, Boulder

Talk online: sachdev.physics.harvard.edu

Outline

1. Introduction to the Hubbard model

   Superexchange and antiferromagnetism

2. Coupled dimer antiferromagnet

   CFT3: the Wilson-Fisher fixed point

3. Honeycomb lattice: semi-metal and antiferromagnetism

   CFT3: Dirac fermions and the Gross-Neveu model

4. Hubbard model as a SU(2) gauge theory

   Spin liquids, valence bond solids: analogies with SQED and SYM

5. Quantum critical dynamics

   AdS/CFT and the collisionless-hydrodynamic crossover

Outline

6. Square lattice: Fermi surfaces and spin density waves

   Fermi pockets and Quantum oscillations

7. Instabilities near the SDW critical point

   d-wave superconductivity and other orders

8. Global phase diagram of the cuprates

   Competition for the Fermi surface

Outline

1. Introduction to the Hubbard model
   Superexchange and antiferromagnetism

2. Coupled dimer antiferromagnet
   CFT3: the Wilson-Fisher fixed point

3. Honeycomb lattice: semi-metal and antiferromagnetism
   CFT3: Dirac fermions and the Gross-Neveu model

4. Hubbard model as a SU(2) gauge theory
   Spin liquids, valence bond solids: analogies with SQED and SYM

5. Quantum critical dynamics
   AdS/CFT and the collisionless-hydrodynamic crossover

The Hubbard Model

$$H = -\sum_{i<j} t_{ij} c^\dagger_{i\alpha} c_{j\alpha} + U \sum_i \left(n_{i\uparrow} - \frac{1}{2} \right) \left(n_{i\downarrow} - \frac{1}{2} \right) - \mu \sum_i c^\dagger_{i\alpha} c_{i\alpha}$$

$t_{ij} \rightarrow$ "hopping". $U \rightarrow$ local repulsion, $\mu \rightarrow$ chemical potential

Spin index $\alpha = \uparrow, \downarrow$

$$n_{i\alpha} = c^\dagger_{i\alpha} c_{i\alpha}$$

$$c^\dagger_{i\alpha} c_{j\beta} + c_{j\beta} c^\dagger_{i\alpha} = \delta_{ij} \delta_{\alpha\beta}$$
$$c_{i\alpha} c_{j\beta} + c_{j\beta} c_{i\alpha} = 0$$

Will study on the honeycomb and square lattices

The Hubbard Model

$$H = -\sum_{i,j} t_{ij} c^\dagger_{i\alpha} c_{j\alpha} + U \sum_i \left(n_{i\uparrow} - \frac{1}{2} \right) \left(n_{i\downarrow} - \frac{1}{2} \right) - \mu \sum_i c^\dagger_{i\alpha} c_{i\alpha}$$

In the limit of large U, and at a density of one particle per site, this maps onto the Heisenberg antiferromagnet

$$H_{AF} = \sum_{i<j} J_{ij} S^a_i S^a_j$$

where $a = x, y, z$,

$$S^a_i = \frac{1}{2} c^{a\dagger}_{i\alpha} \sigma^a_{\alpha\beta} c_{i\beta},$$

with σ^a the Pauli matrices and

$$J_{ij} = \frac{4t^2_{ij}}{U}$$

therefore always appropriate, and only the critical point $g = g_c$ has genuinely different properties at $T = 0$.

5.1 Effective Hamiltonian method

We consider a Hamiltonian of the form $H = H_0 + H_1$, where the eigenstates of H_0 are easily determined, and we are interested in describing the influence of H_1 in perturbation theory. Further, we assume that the eigenvalues of H_0 are separated into distinct groups of closely-spaced levels, such that the energy separation between two levels within the same group is always much smaller than the separation between two levels in distinct groups. We use the symbols $\alpha, \beta, \ldots$ to denote the groups, and $i, j, \ldots$ to denote levels within each group. Thus the eigenstates of H_0 are $|i, \alpha\rangle$, with eigenenergies $E_{i\alpha}$, and so

$$|E_{i\alpha} - E_{j\alpha}| \ll |E_{i\alpha} - E_{j\beta}| \quad \text{for } \alpha \neq \beta \tag{5.2}$$

We are often interested in the structure of the levels within a given group, and would like to understand their behavior without reference to levels in other groups. However, in general, H_1 will have non-zero matrix elements between states belonging to different groups: consequently a conventional perturbative analysis will require repeated reference to states lying outside the group of interest. The idea of the effective Hamiltonian method is to perform a unitary transformation which eliminates these inter-group matrix elements. After the unitary transformation, we will obtain a new Hamiltonian H_{eff} which has non-zero matrix elements only within each group.

We skip the straightforward, but tedious, analysis needed to obtain H_{eff} order-by-order in H_1. We only quote here the final result to second order in H_1. The new Hamiltonian H_{eff} is defined by the following non-zero matrix elements between any two levels, $|i, \alpha\rangle$ and $|j, \alpha\rangle$ belonging to the same group α:

$$\begin{aligned} &\langle i, \alpha | H_{\text{eff}} | j, \alpha \rangle = E_{i\alpha}\delta_{ij} + \langle i, \alpha | H_1 | j, \alpha \rangle + \\ &\sum_{k, \beta \neq \alpha} \frac{\langle i, \alpha | H_1 | k, \beta \rangle \langle k, \beta | H_1 | j, \alpha \rangle}{2} \left(\frac{1}{E_{i\alpha} - E_{k\beta}} + \frac{1}{E_{j,\alpha} - E_{k\beta}} \right) \end{aligned} \tag{5.3}$$

Naturally, we have $\langle i, \alpha | H_{\text{eff}} | j, \beta \rangle = 0$ for all $\alpha \neq \beta$, ensuring that H_{eff} is block diagonal, and we can work independently within each group α.

Hubbard Model and Superexchange

$$H = -t \sum_{\langle ij \rangle} \left(c^{+}_{i\sigma} c_{j\sigma} + c^{+}_{j\sigma} c_{i\sigma} \right)$$

$$- \mu \sum_{i} c^{+}_{i\sigma} c_{i\sigma}$$

$$+ U \sum_{i} n_{i\uparrow} n_{i\downarrow}$$

Take 2 sites and 2 electrons.

$U \gg t$.

6 states

$|1\rangle = c^{+}_{1\uparrow} c^{+}_{2\uparrow} |0\rangle \qquad E_0 = 0$

$|2\rangle = c^{+}_{1\uparrow} c^{+}_{2\downarrow} |0\rangle \qquad E_0 = 0$

$|3\rangle = c^{+}_{1\downarrow} c^{+}_{2\uparrow} |0\rangle \qquad E_0 = 0$

$|4\rangle = c^{+}_{1\downarrow} c^{+}_{2\downarrow} |0\rangle \qquad E_0 = 0$

$|5\rangle = c^{+}_{1\uparrow} c^{+}_{1\downarrow} |0\rangle \qquad E_0 = U$

$|6\rangle = c^{+}_{2\uparrow} c^{+}_{2\downarrow} |0\rangle \qquad E_0 = U.$

Eliminate states $|5\rangle$ and $|6\rangle$
by effective Hamiltonian method.

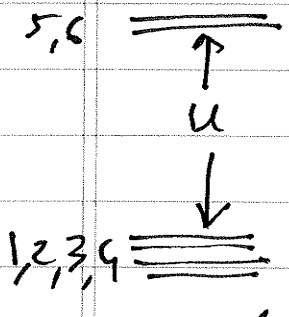

$$H_0 = U(n_{1\uparrow} n_{1\downarrow} + n_{2\uparrow} n_{2\downarrow})$$

$$H_1 = -t(c^+_{1\uparrow} c_{2\uparrow} + c^+_{1\downarrow} c_{2\downarrow} + c^+_{2\uparrow} c_{1\uparrow} + c^+_{2\downarrow} c_{1\downarrow})$$

Non-zero matrix elements

~~$\langle 6|H_1|2\rangle$~~

$$\langle 6|H_1|2\rangle = -t$$

$$\langle 5|H_1|2\rangle = -t$$

$$\langle 6|H_1|3\rangle = t$$

$$\langle 5|H_1|3\rangle = t.$$

So

$$\langle 2|H_{eff}|2\rangle = -\frac{2t^2}{U} = \langle 3|H_{eff}|3\rangle$$

$$\langle 2|H_{eff}|3\rangle = \frac{2t^2}{U} = \langle 3|H_{eff}|2\rangle.$$

So to order t^2/u.

$|1\rangle \longrightarrow E = 0$

$|4\rangle \longrightarrow E = 0$.

States $|2\rangle$ and $|3\rangle$

$$H_{eff} = \begin{pmatrix} -2t^2/u & 2t^2/u \\ 2t^2/u & -2t^2/u \end{pmatrix} \longrightarrow E = 0, -\frac{4t^2}{u}.$$

Energy levels

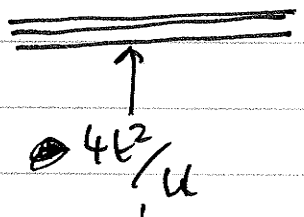

$|\uparrow\uparrow\rangle$, $|\downarrow\downarrow\rangle$, $\dfrac{|\uparrow\downarrow\rangle + |\downarrow\uparrow\rangle}{\sqrt{2}}$

$4t^2/u$

$\dfrac{|\uparrow\downarrow\rangle - |\downarrow\uparrow\rangle}{\sqrt{2}}$.

Equivalent to $H_{eff} = J\,\vec{S}_1 \cdot \vec{S}_2$

where $J = 4t^2/u$.

Outline

1. Introduction to the Hubbard model

   Superexchange and antiferromagnetism

2. Coupled dimer antiferromagnet

   CFT3: the Wilson-Fisher fixed point

3. Honeycomb lattice: semi-metal and antiferromagnetism

   CFT3: Dirac fermions and the Gross-Neveu model

4. Hubbard model as a SU(2) gauge theory

   Spin liquids, valence bond solids: analogies with SQED and SYM

5. Quantum critical dynamics

   AdS/CFT and the collisionless-hydrodynamic crossover

Outline

1. Introduction to the Hubbard model

   Superexchange and antiferromagnetism

2. Coupled dimer antiferromagnet

   CFT3: the Wilson-Fisher fixed point

3. Honeycomb lattice: semi-metal and antiferromagnetism

   CFT3: Dirac fermions and the Gross-Neveu model

4. Hubbard model as a SU(2) gauge theory

   Spin liquids, valence bond solids: analogies with SQED and SYM

5. Quantum critical dynamics

   AdS/CFT and the collisionless-hydrodynamic crossover

Square lattice antiferromagnet

$$H = \sum_{\langle ij \rangle} J_{ij} \vec{S}_i \cdot \vec{S}_j$$

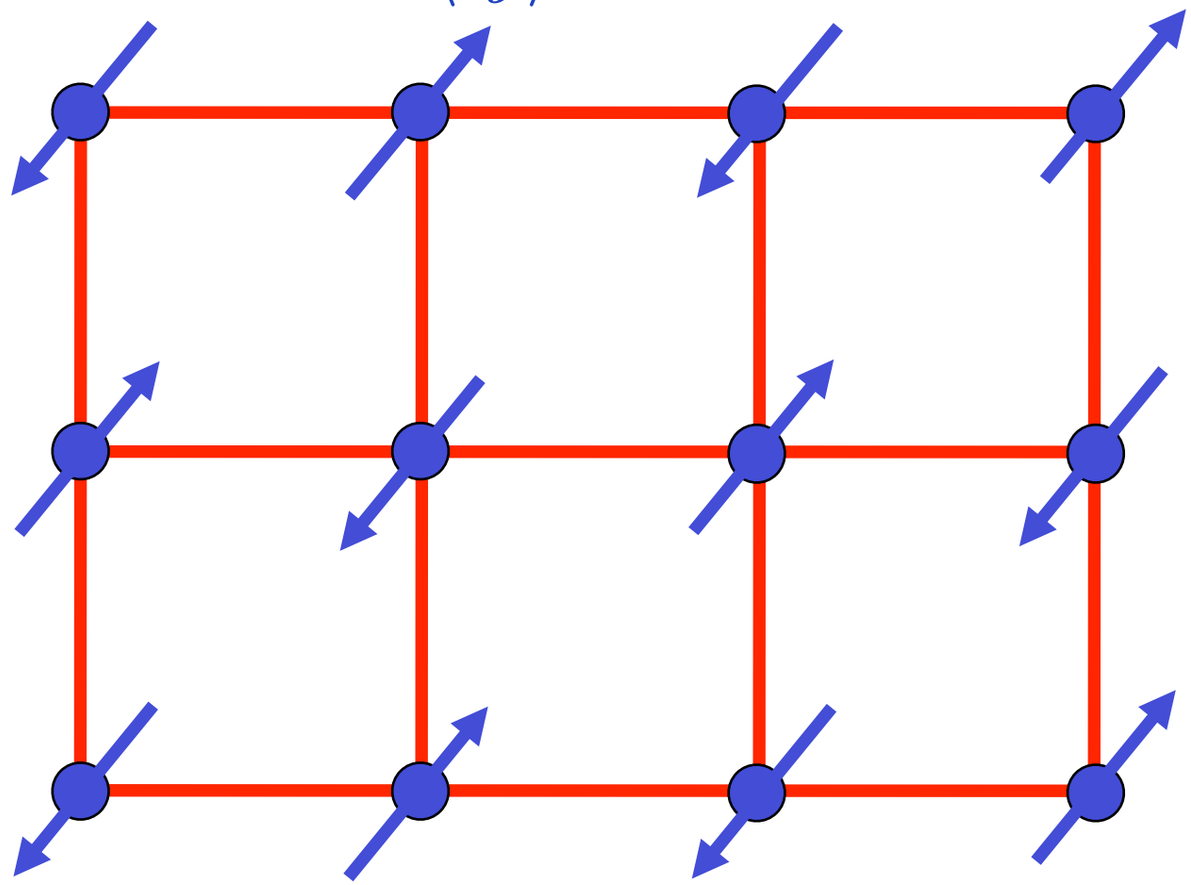

Ground state has long-range Néel order

Order parameter is a single vector field $\vec{\varphi} = \eta_i \vec{S}_i$

$\eta_i = \pm 1$ on two sublattices

$\langle \vec{\varphi} \rangle \neq 0$ in Néel state.

Square lattice antiferromagnet

$$H = \sum_{\langle ij \rangle} J_{ij} \vec{S}_i \cdot \vec{S}_j$$

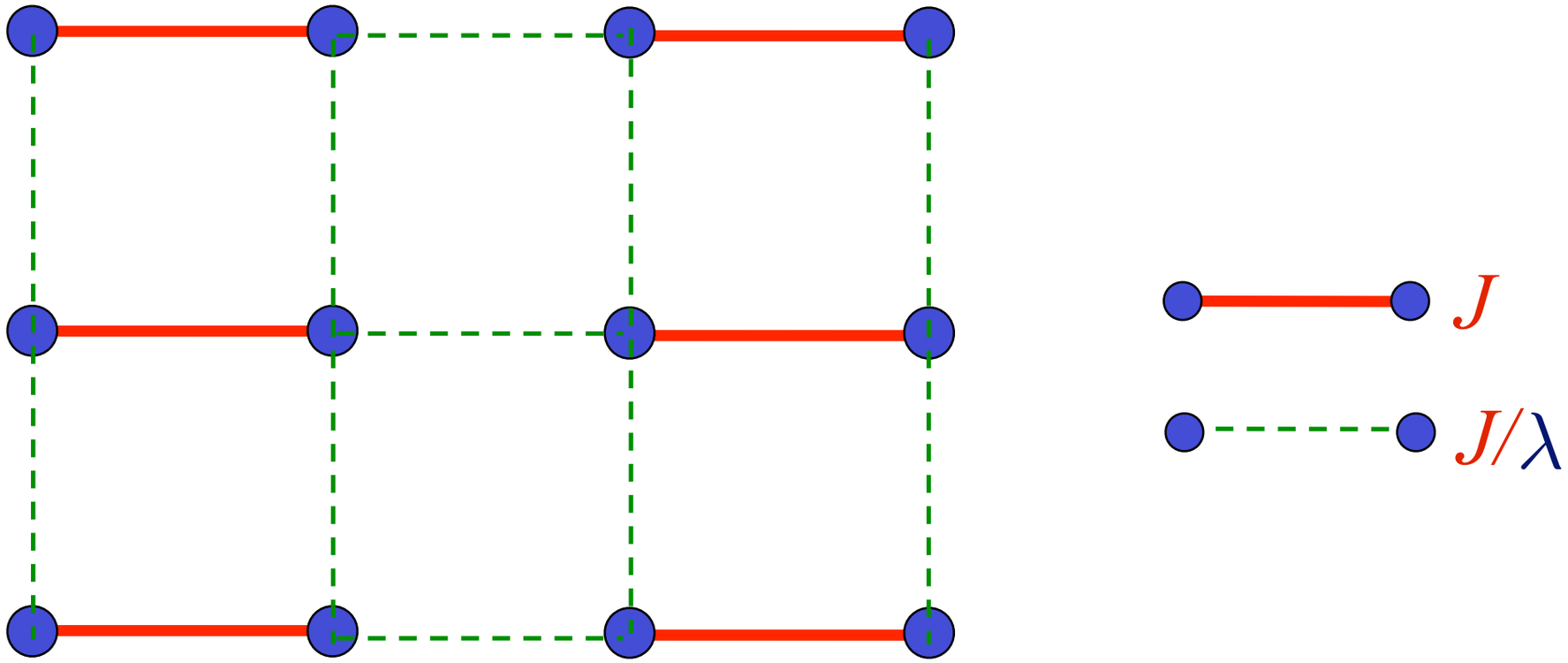

Weaken some bonds to induce spin entanglement in a new quantum phase

Square lattice antiferromagnet

$$H = \sum_{\langle ij \rangle} J_{ij} \vec{S}_i \cdot \vec{S}_j$$

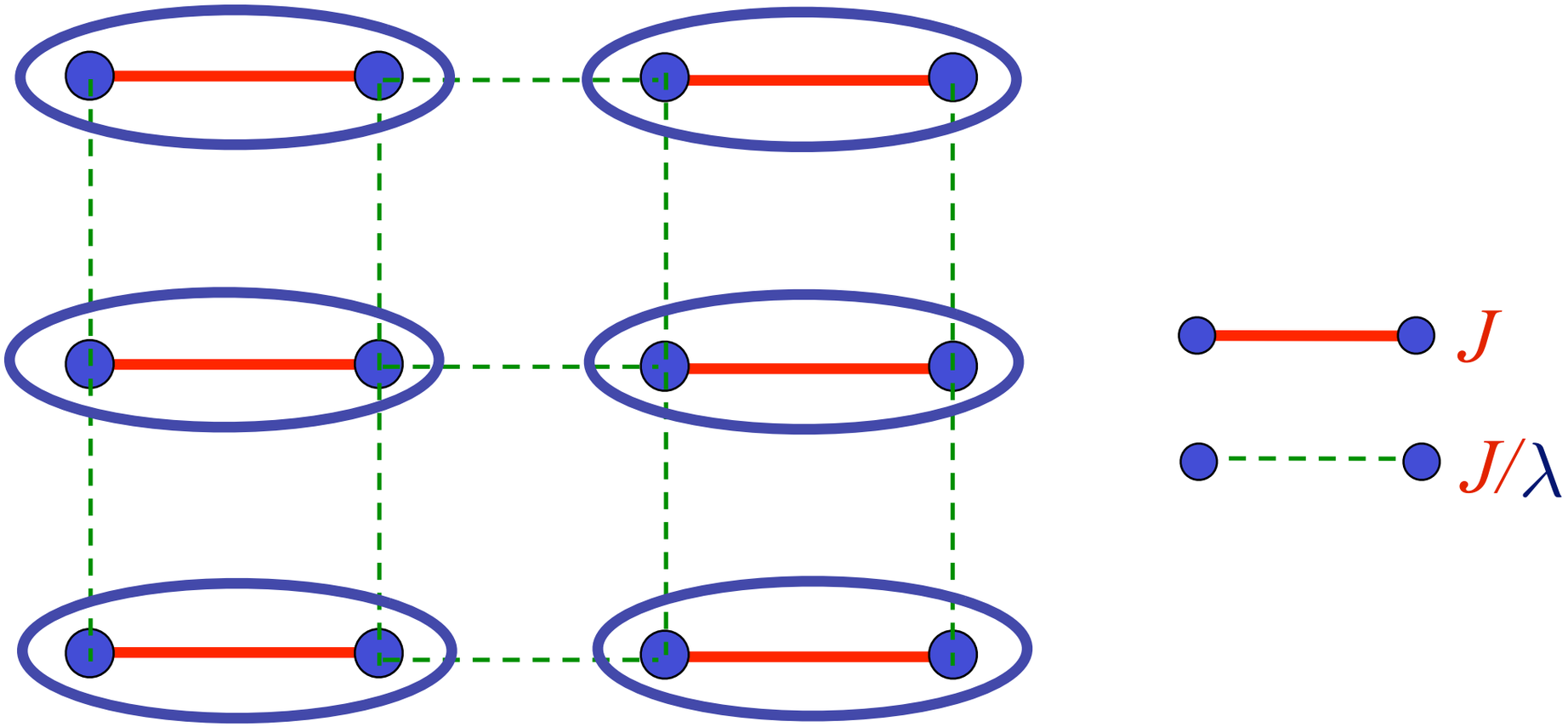

Ground state is a "quantum paramagnet"
with spins locked in valence bond singlets

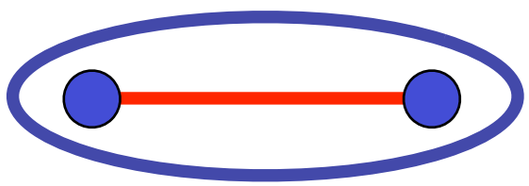

$$= \frac{1}{\sqrt{2}} \left(\left| \uparrow\downarrow \right\rangle - \left| \downarrow\uparrow \right\rangle \right)$$

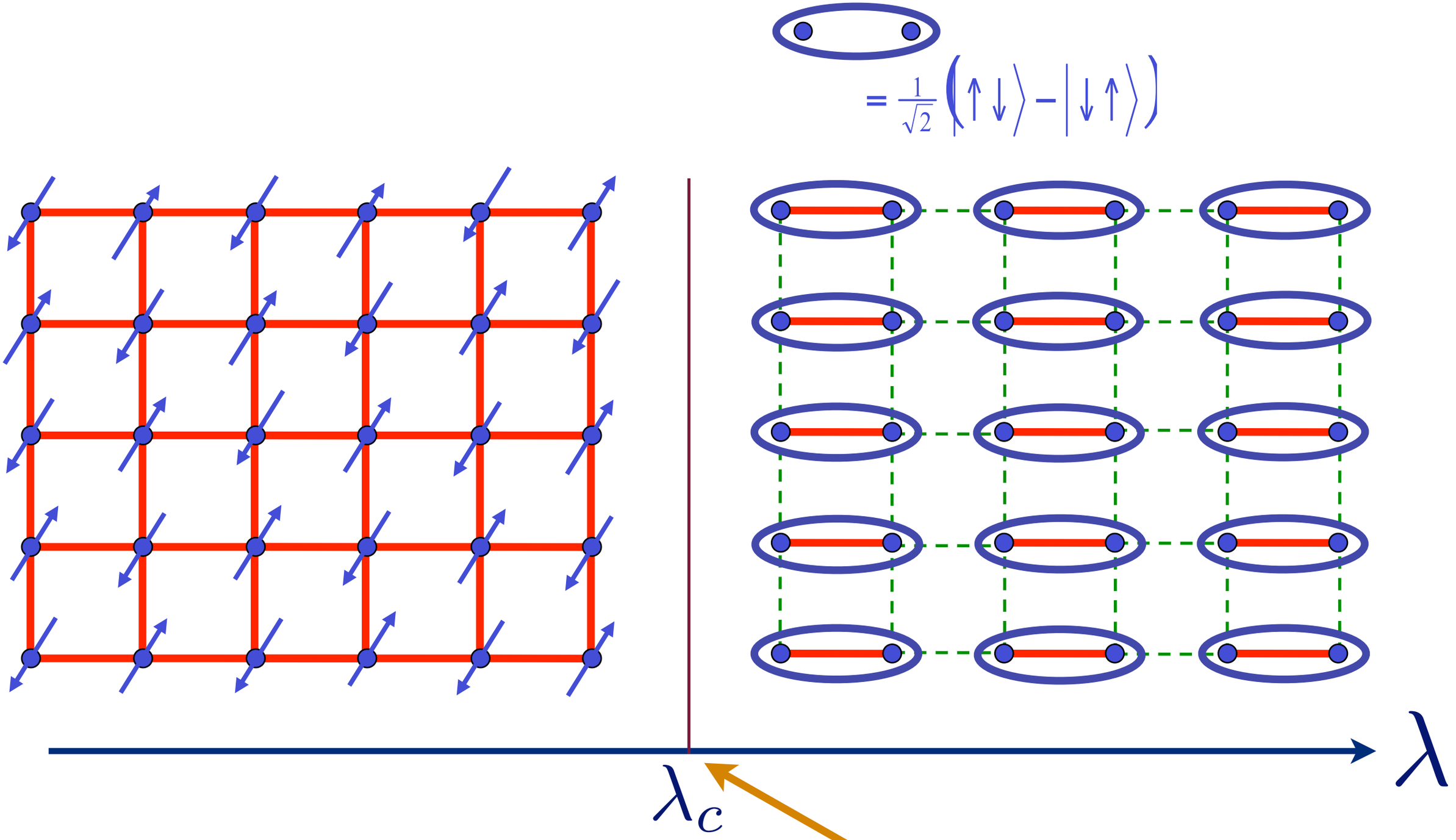

Quantum critical point with non-local entanglement in spin wavefunction

M. Matsumoto, C. Yasuda, S. Todo, and H. Takayama, *Phys. Rev.* B **65**, 014407 (2002).

Excitation spectrum in the paramagnetic phase

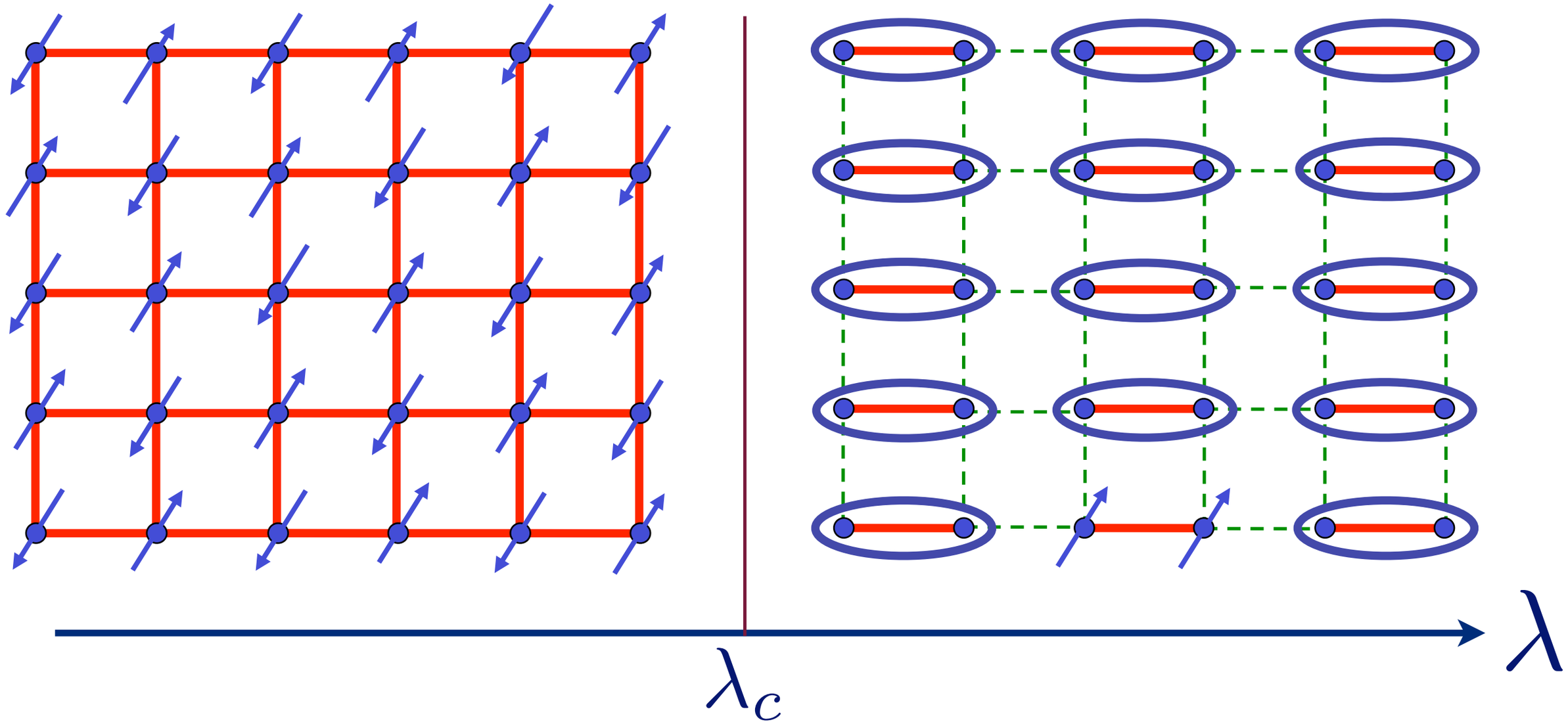

Excitation spectrum in the paramagnetic phase

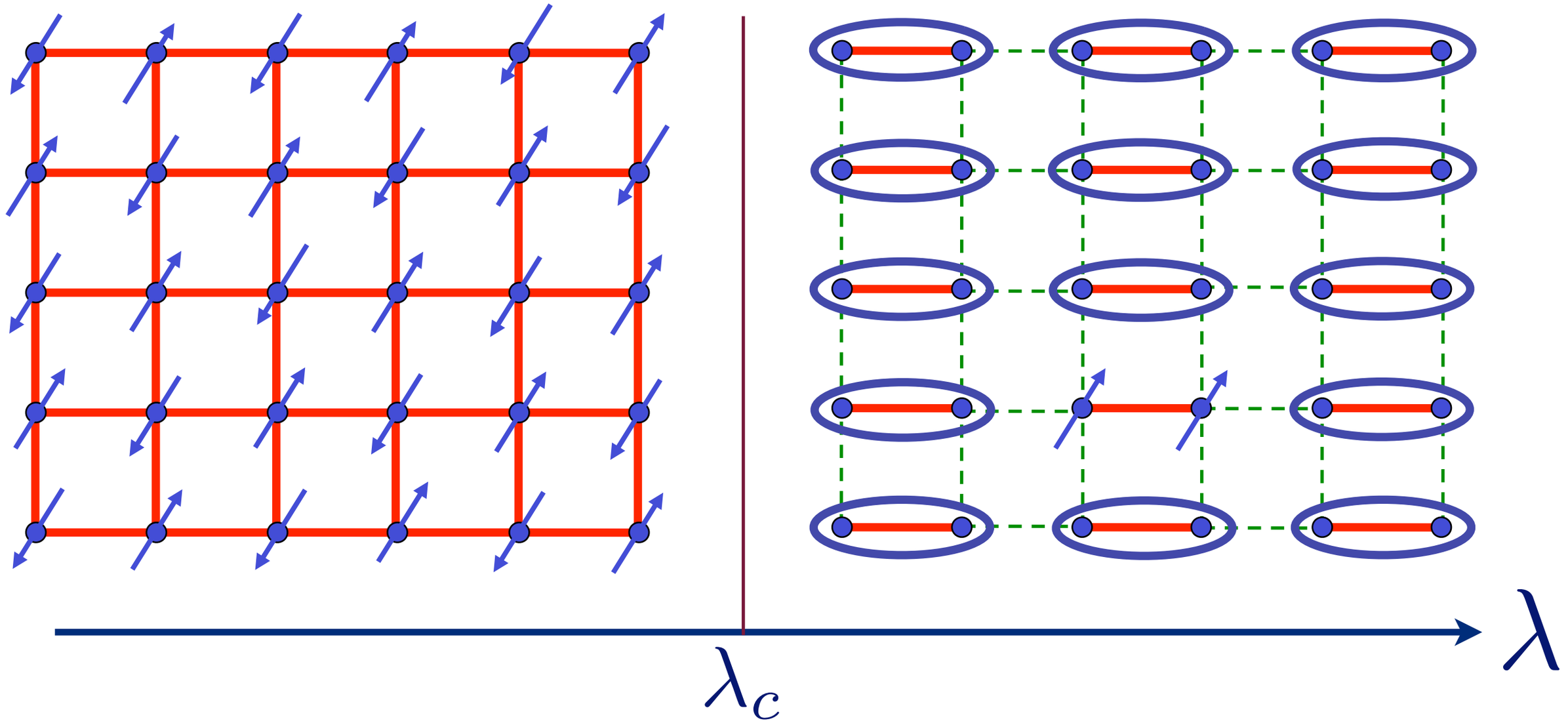

Excitation spectrum in the paramagnetic phase

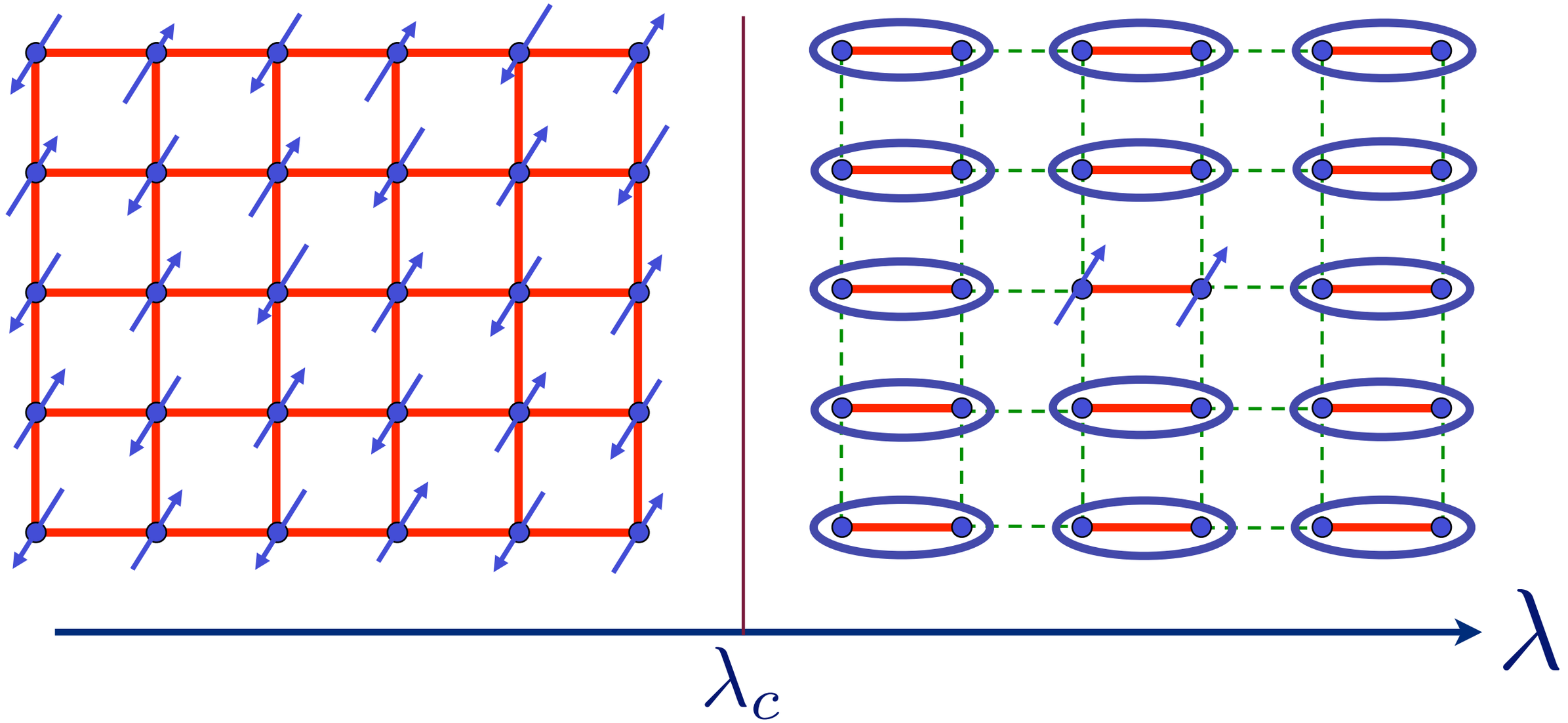

Excitation spectrum in the paramagnetic phase

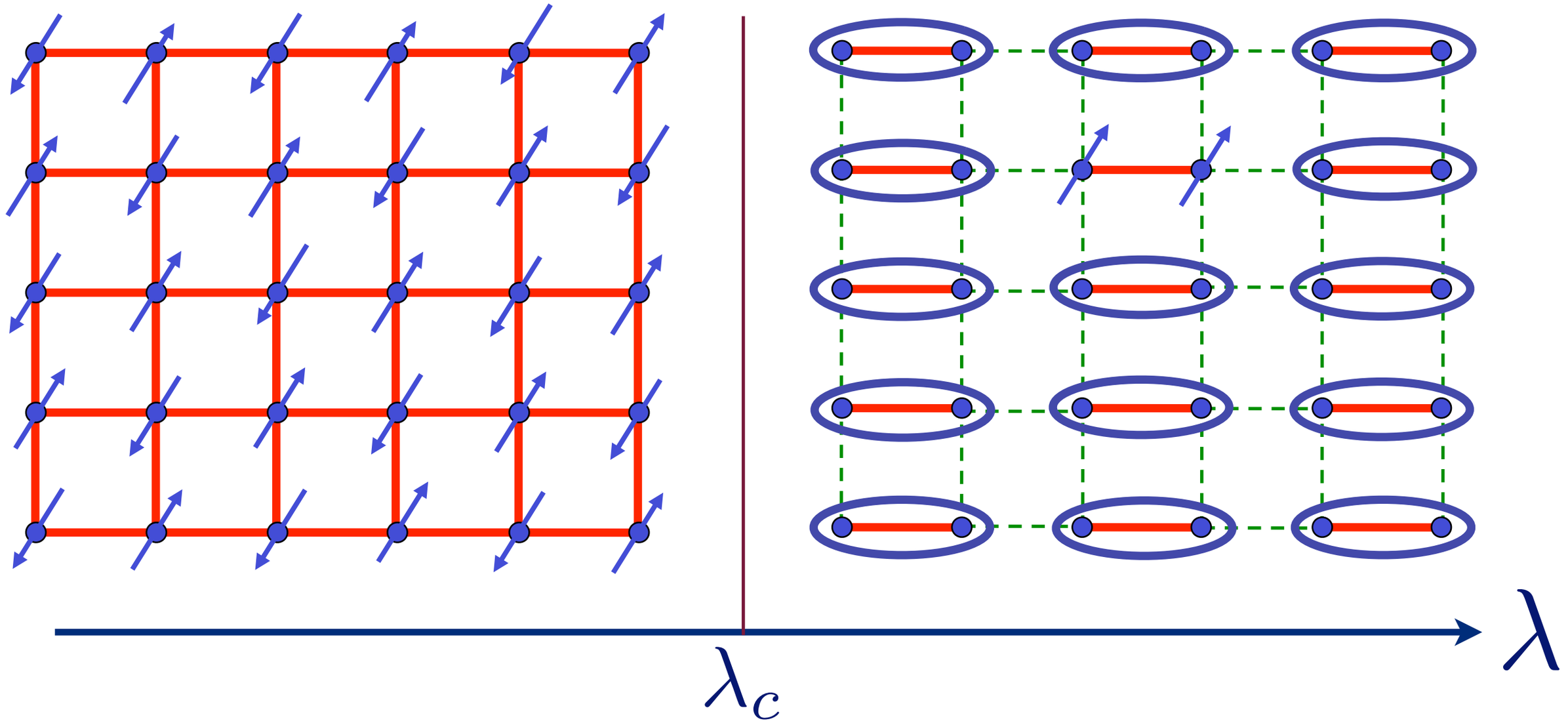

Excitation spectrum in the paramagnetic phase

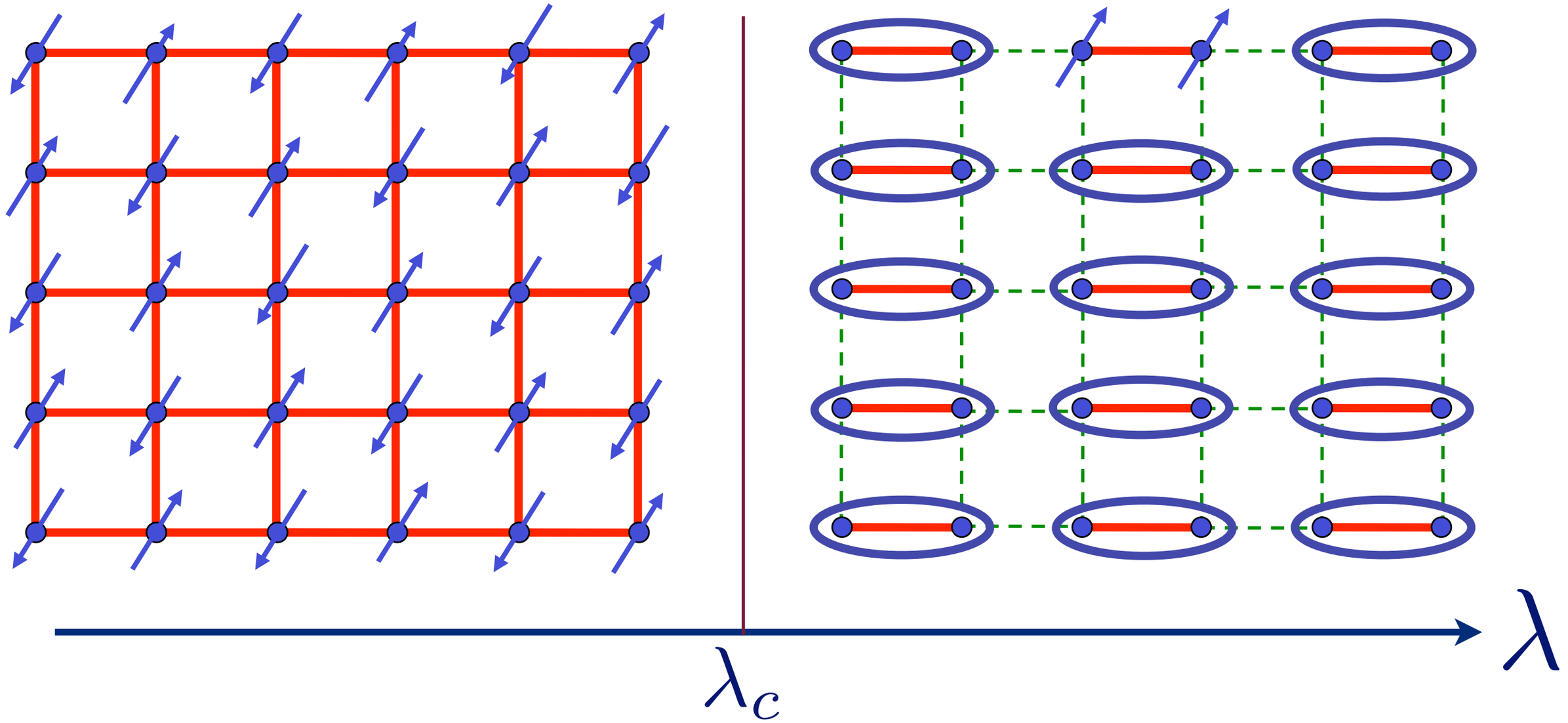

Sharp spin 1 particle excitation above an energy gap (spin gap)

Excitation spectrum in the Néel phase

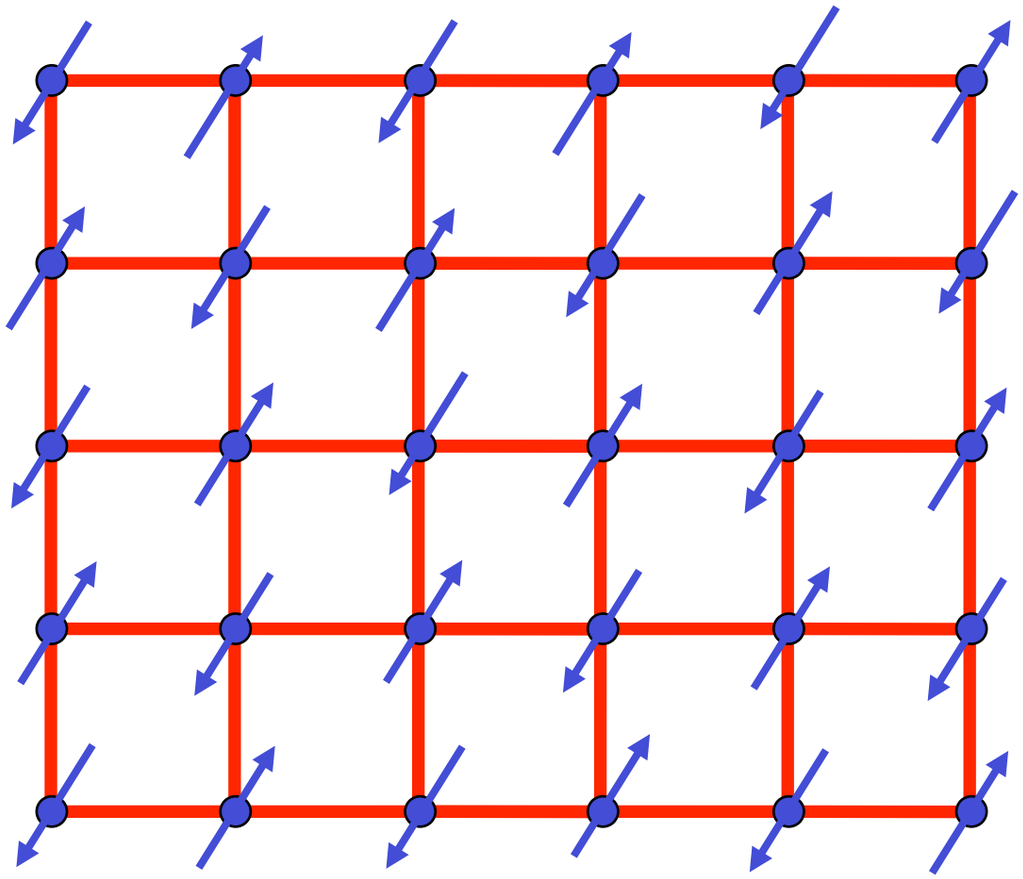

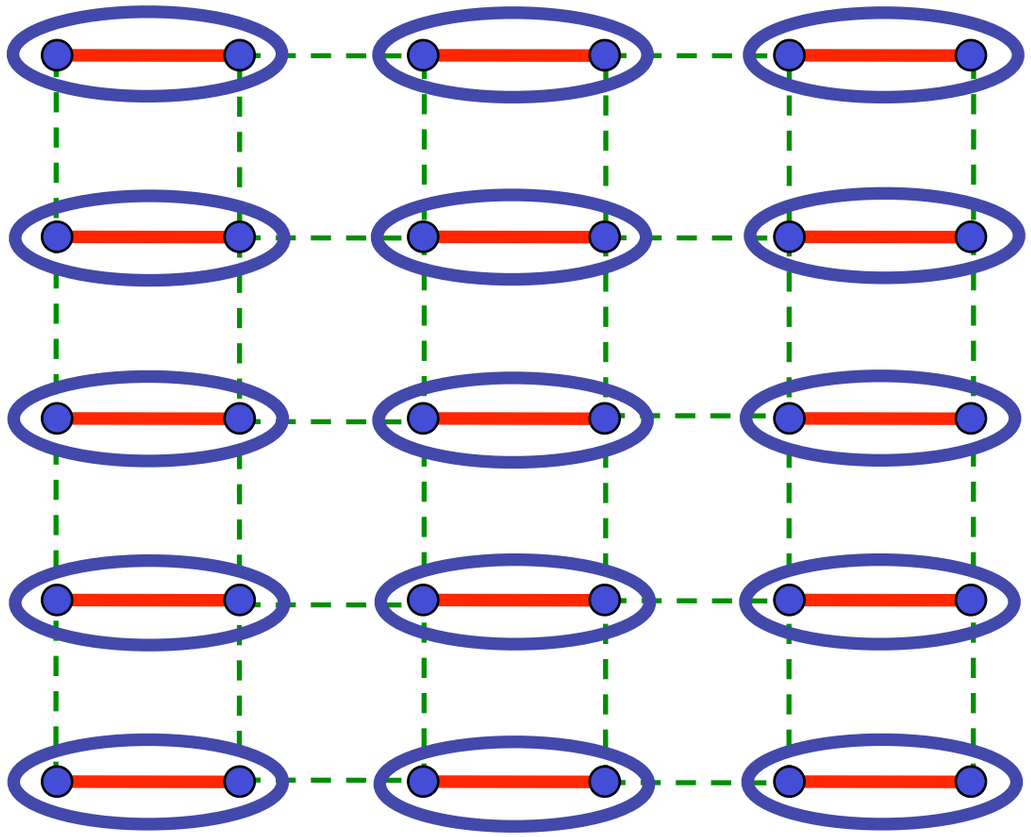

λ_c

λ

Excitation spectrum in the Néel phase

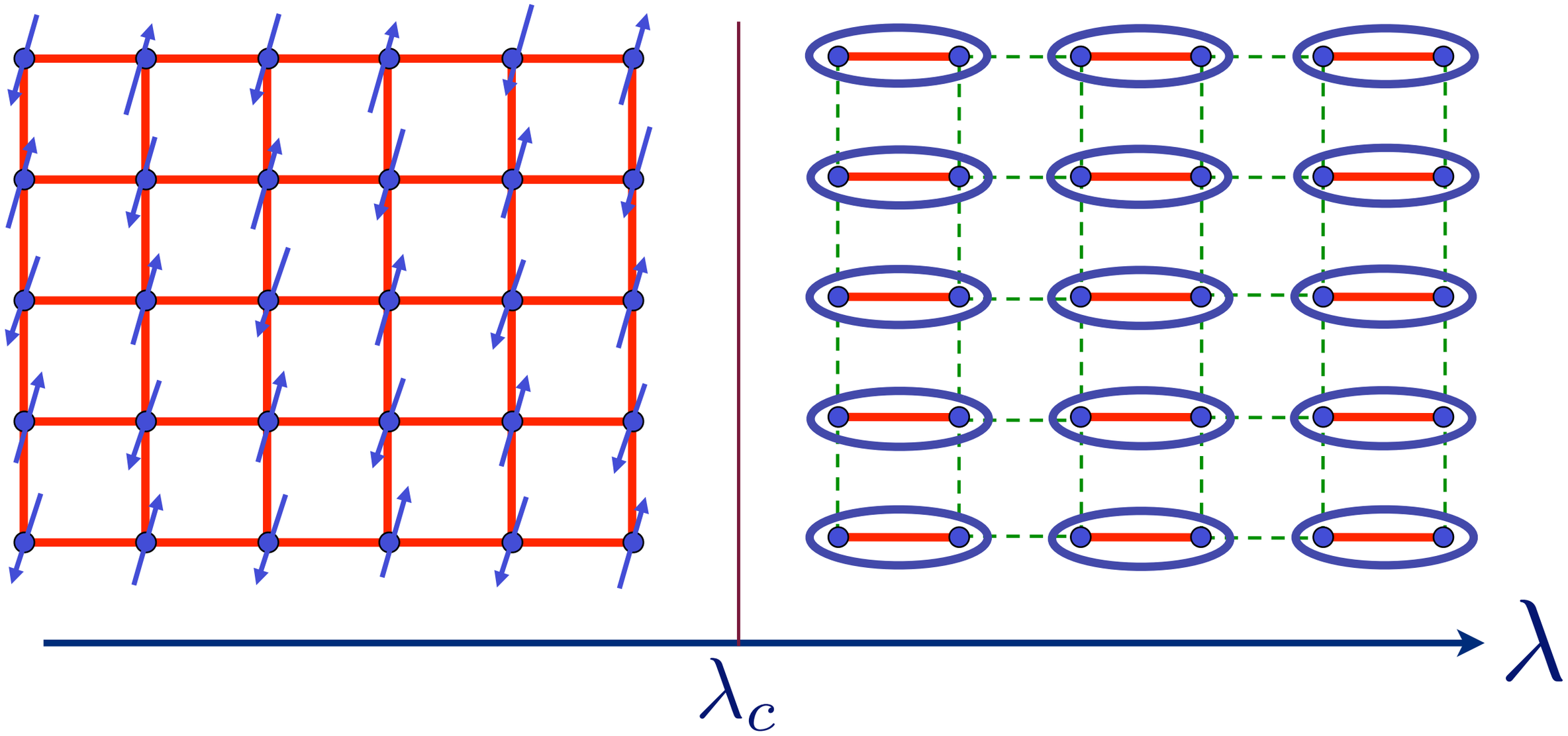

Spin waves

Excitation spectrum in the Néel phase

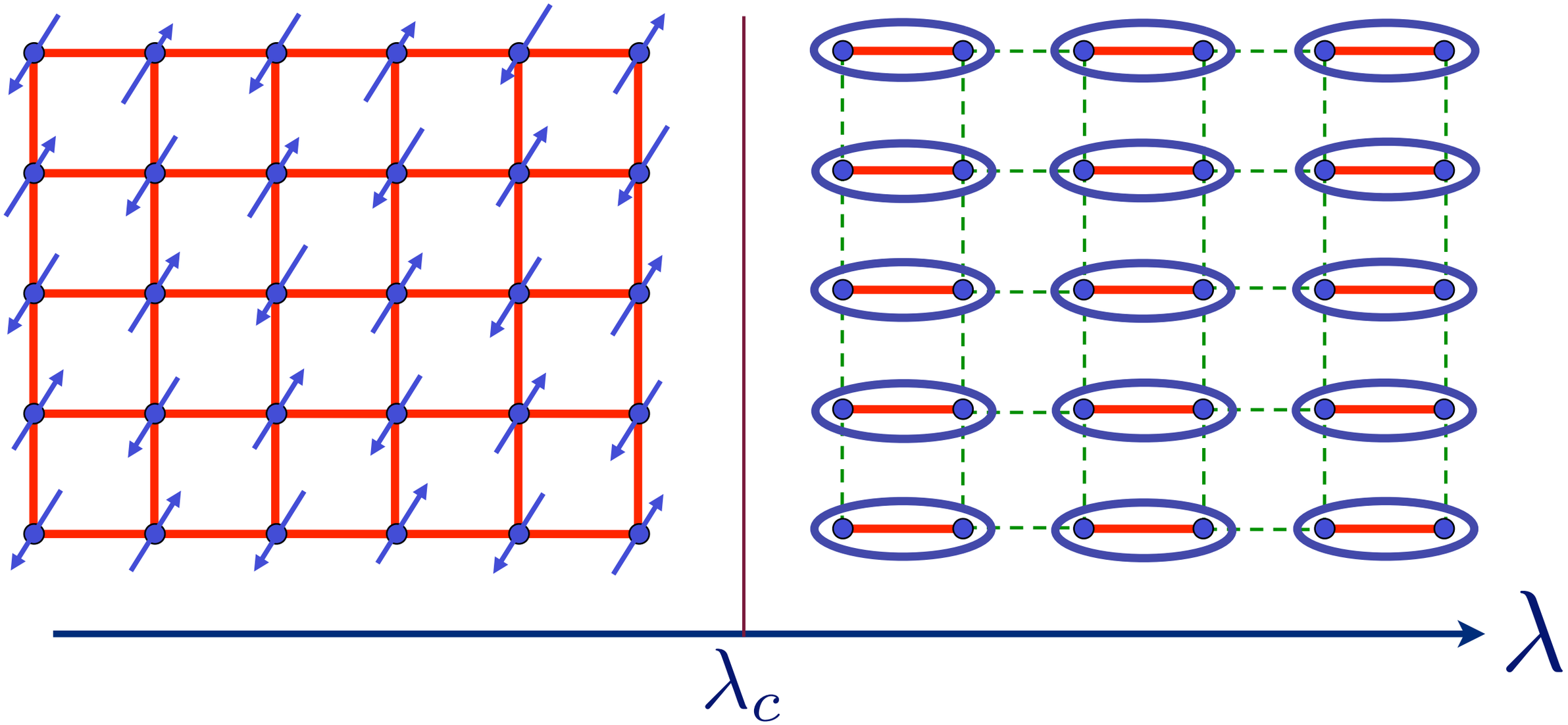

Spin waves

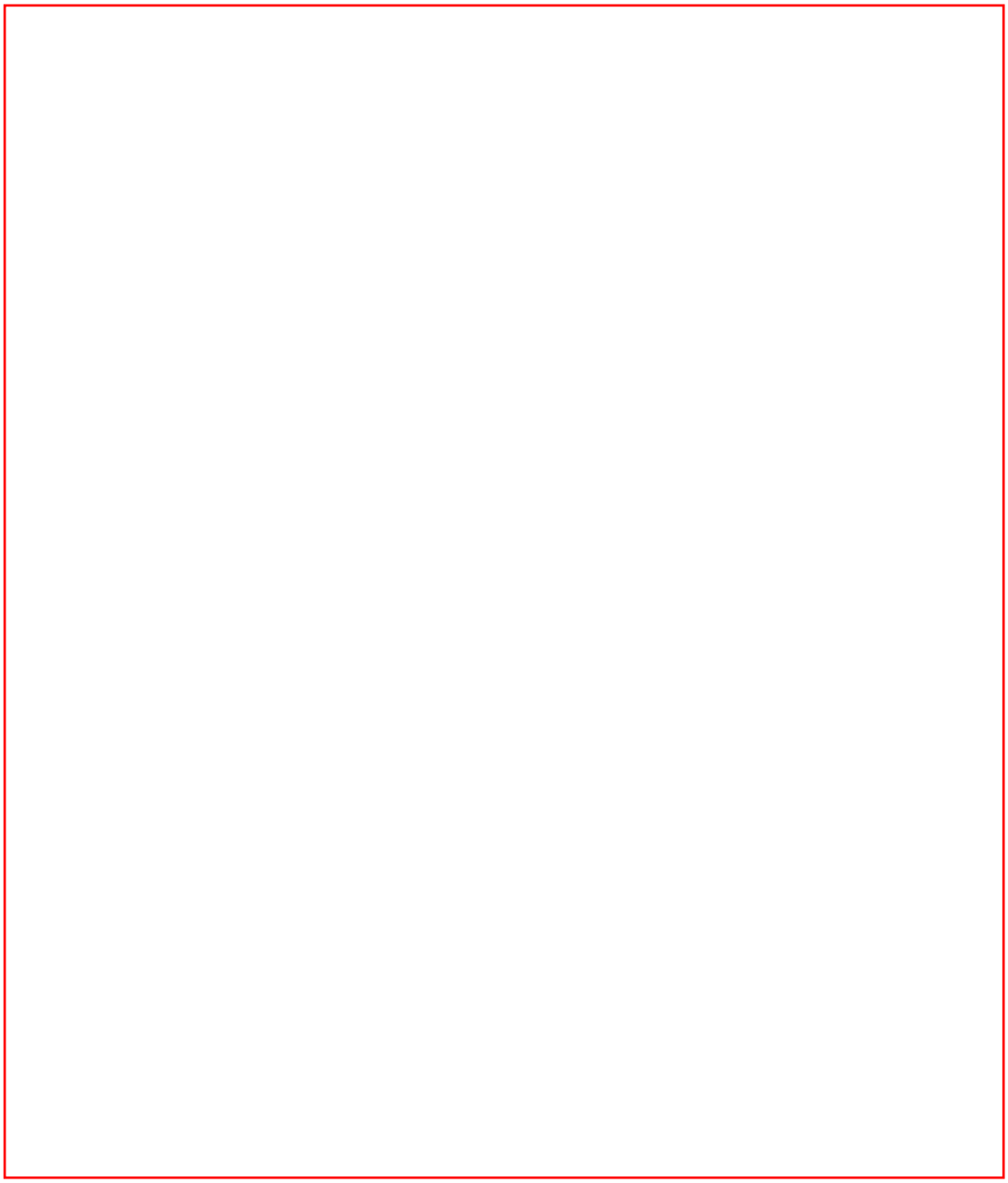

1.4.2 Quantum Rotor Model

We turn to the somewhat less familiar quantum rotor models. Elementary quantum rotors do not exist in nature; rather, each quantum rotor is an effective quantum degree of freedom for the low energy states of a small number of electrons or atoms. We will first define the quantum mechanics of a single rotor and then turn to the lattice quantum rotor model. The connection to the experimental models introduced in Section 1.3 will be

described below in Section 1.4.3. Further details of this connection appear in Chapters 9, 19.

Each rotor can be visualized as a particle constrained to move on the surface of a (fictitious) ($N > 1$)-dimensional sphere. The orientation of each rotor is represented by an N-component unit vector $\hat{\mathbf{n}}_i$ which satisfies

$$\hat{\mathbf{n}}^2 = 1. \tag{1.14}$$

The caret on $\hat{\mathbf{n}}_i$ reminds us that the orientation of the rotor is a quantum mechanical operator, while i represents the site on which the rotor resides; we will shortly consider an infinite number of such rotors residing on the sites of a d-dimensional lattice. Each rotor has a momentum $\hat{\mathbf{p}}_i$, and the constraint (1.14) implies that this must be tangent to the surface of the N-dimensional sphere. The rotor position and momentum satisfy the usual commutation relations

$$[\hat{n}_\alpha, \hat{p}_\beta] = i\delta_{\alpha\beta} \tag{1.15}$$

on each site i; here $\alpha, \beta = 1 \ldots N$. (Here, and in the remainder of the book, we will always measure time in units in which

$$\hbar = 1, \tag{1.16}$$

unless stated explicitly otherwise. This is also a good point to note that we will also set Boltzmann's constant

$$k_B = 1 \tag{1.17}$$

by absorbing it into the units of temperature, T.) We will actually find it more convenient to work with the $N(N-1)/2$ components of the rotor angular momentum

$$\hat{L}_{\alpha\beta} = \hat{n}_\alpha \hat{p}_\beta - \hat{n}_\beta \hat{p}_\alpha. \tag{1.18}$$

These operators are the generators of the group of rotation in N dimensions, denoted O(N). Their commutation relations follow straightforwardly from (1.15) and (1.18). The case $N = 3$ will be of particular interest to us: For this we define $\hat{L}_\alpha = (1/2)\epsilon_{\alpha\beta\gamma} L_{\beta\gamma}$ (where $\epsilon_{\alpha\beta\gamma}$ is a totally antisymmetric tensor with $\epsilon_{123} = 1$), and then the commutation relation between the operators on each site are

$$\begin{aligned} [\hat{L}_\alpha, \hat{L}_\beta] &= i\epsilon_{\alpha\beta\gamma}\hat{L}_\gamma, \\ [\hat{L}_\alpha, \hat{n}_\beta] &= i\epsilon_{\alpha\beta\gamma}\hat{n}_\gamma, \\ [\hat{n}_\alpha, \hat{n}_\beta] &= 0; \end{aligned} \tag{1.19}$$

the operators with different site labels all commute.

The dynamics of each rotor is governed simply by its kinetic energy term; interesting effects will arise from potential energy terms that couple the rotors together, and these will be considered momentarily. Each rotor has the kinetic energy

$$H_K = \frac{J\tilde{g}}{2}\hat{\mathbf{L}}^2, \tag{1.20}$$

where $1/J\tilde{g}$ is the rotor moment of inertia (we have put a tilde over g as we wish to reserve g for a different coupling to be introduced below). The Hamiltonian H_K can be readily diagonalized for general values of N by well-known group theoretical methods. We quote the results for the physically important cases of $N = 2$ and 3. For $N = 2$ the eigenvalues are

$$J\tilde{g}\ell^2/2 \qquad \ell = 0, 1, 2, \ldots; \quad \text{degeneracy} = 2 - \delta_{\ell,0}. \tag{1.21}$$

Note that there is a nondegenerate ground state with $\ell = 0$, while all excited states are two-fold degenerate, corresponding to a left- or right-moving rotor. This spectrum will be important in the mapping to physical models to be discussed in Section 1.4.3. For $N = 3$, the eigenvalues of H_K are

$$J\tilde{g}\ell(\ell+1)/2 \qquad \ell = 0, 1, 2, \ldots; \quad \text{degeneracy} = 2\ell + 1, \tag{1.22}$$

corresponding to the familiar angular momentum states in three dimensions. These states can be viewed as representing the eigenstates of an even number of antiferromagnetically coupled Heisenberg spins, as will be discussed more explicitly in Section 1.4.3 and in Chapter 19, where will see that there is a general and powerful correspondence between quantum antiferromagnets and $N = 3$ rotors.

We are ready to write down the full quantum rotor Hamiltonian, which shall be the focus of intensive study in Parts II and III. We place a single quantum rotor on the sites, i, of a d-dimensional lattice, obeying the Hamiltonian

$$H_R = \frac{J\tilde{g}}{2}\sum_i \hat{\mathbf{L}}_i^2 - J\sum_{\langle ij\rangle} \hat{\mathbf{n}}_i \cdot \hat{\mathbf{n}}_j. \tag{1.23}$$

We have augmented the sum of kinetic energies of each site with a coupling, J, between rotor orientations on neighboring sites. This coupling energy is minimized by the simple "magnetically ordered" state in which all the rotors are oriented in the same direction. In contrast, the rotor kinetic energy is minimized when the orientation of the rotor is maximally uncertain (by the uncertainty principle), and so the first term in H_R prefers a quantum paramagnetic state in which the rotors do not have a definite orientation (i.e., $\langle \mathbf{n} \rangle = 0$). Thus the roles of the two terms in H_R closely parallel those

of the terms in the Ising model H_I. As in Section 1.4.1, for $\tilde{g} \gg 1$, when the kinetic energy dominates, we expect a quantum paramagnet in which, following (1.9),

$$\langle 0|\hat{\mathbf{n}}_i \cdot \hat{\mathbf{n}}_j|0\rangle \sim e^{-|x_i - x_j|/\xi}. \tag{1.24}$$

Similarly, for $\tilde{g} \ll 1$, when the coupling term dominates, we expect a magnetically ordered state in which, as in (1.12),

$$\lim_{|x_i - x_j| \to \infty} \langle 0|\hat{\mathbf{n}}_i \cdot \hat{\mathbf{n}}_j|0\rangle = N_0^2. \tag{1.25}$$

Finally, we can anticipate a second-order quantum phase transition between the two phases at $\tilde{g} = \tilde{g}_c$, and the behavior of N_0 and ξ upon approaching this point will be similar to that in the Ising case. These expectations turn out to be correct for $d > 1$, but we will see that they need some modifications for $d = 1$. In one dimension, we will show that $\tilde{g}_c = 0$ for $N \geq 3$, and so the ground state is a quantum paramagnetic state for all nonzero $\tilde{g}$. The case $N = 2$, $d = 1$ is special: There is a transition at a finite $\tilde{g}_c$, but the divergence of the correlation length does not obey (1.2) and the long-distance behavior of the correlation function $\tilde{g} < \tilde{g}_c$ differs from (1.25). This case will not be considered until Section 20.3 in Part III.

1.4.3 Physical realizations of quantum rotors

We will consider the $N = 3$ quantum rotors first, and expose a simple and important connection between O(3) quantum rotor models and a certain class of "dimerized" antiferromagnets, of which $TlCuCl_3$ is the example we highlighted in Section 1.3. Actually the connection between rotor models and antiferromagnets is far more general than the present discussion may suggest, as we will see later in Chapter 19. However, this discussion should enable the reader to gain an intuitive feeling for the physical interpretation of the degrees of freedom of the rotor model.

Consider a dimerized system of "Heisenberg spins" $\hat{\mathbf{S}}_{1i}$ and $\hat{\mathbf{S}}_{2i}$, where i now labels a pair of spins (a 'dimer'). Their Hamiltonian is

$$H_d = K \sum_i \hat{\mathbf{S}}_{1i} \cdot \hat{\mathbf{S}}_{2i} + J \sum_{\langle ij \rangle} \left(\hat{\mathbf{S}}_{1i} \cdot \hat{\mathbf{S}}_{1j} + \hat{\mathbf{S}}_{2i} \cdot \hat{\mathbf{S}}_{2j} \right). \tag{1.26}$$

The $\hat{\mathbf{S}}_{ni}$ ($n = 1, 2$ labels the spins within a dimer) are spin operators usually representing the total spin of a set of electrons in some localized atomic states. See Fig 1.3. On each site, the spins $\hat{\mathbf{S}}_{ni}$ obey the angular momentum

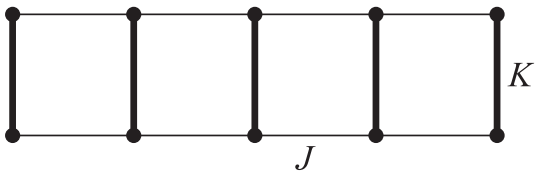

Figure 1.3 A dimerized quantum spin system. Spins with angular momentum S reside on the circles, with antiferromagnetic exchange couplings as shown.

commutation relations

$$\left[\hat{S}_\alpha, \hat{S}_\beta\right] = i\epsilon_{\alpha\beta\gamma}\hat{S}_\gamma \tag{1.27}$$

(the site index has been dropped above), while spin operators on different sites commute. These commutation relations are the same as those of the $\hat{\mathbf{L}}$ operators in (1.19). However, there is one crucial difference between Hilbert space of states on which the quantum rotors and Heisenberg spins act. For the rotor models we allowed states with arbitrary total angular momentum ℓ on each site, as in (1.22), and so there were an infinite number of states on each site. For the present Heisenberg spins, however, we will only allow states with total spin S on each site, and we will permit S to be integer or half-integer. Thus there are precisely $2S + 1$ states on each site

$$|S, m\rangle \quad \text{with } m = -S \ldots S, \tag{1.28}$$

and the operator identity

$$\hat{\mathbf{S}}_{ni}^2 = S(S+1) \tag{1.29}$$

holds for each i and n. In addition to describing $TlCuCl_3$, Hamiltonians like H_d describe spin-ladder compounds in $d = 1$ [39, 131] and "double layer" antiferromagnets in the family of the high-temperature superconductors in $d = 2$ [581, 582, 387, 402, 517, 518, 159].

Let us examine the properties of H_d in the limit $K \gg J$. As a first approximation, we can neglect the J couplings entirely, and then H_d splits into decoupled pairs of sites, each with a strong antiferromagnetic coupling K between two spins. The Hamiltonian for each pair can be diagonalized by noting that $\mathbf{S}_{1i}$ and $\mathbf{S}_{2i}$ couple into states with total angular momentum $0 \leq \ell \leq 2S$, and so we obtain the eigenenergies

$$(K/2)(\ell(\ell+1) - 2S(S+1)), \qquad \text{degeneracy } 2\ell + 1. \tag{1.30}$$

Note that these energies and degeneracies are in one-to-one correspondence with those of a single quantum rotor in (1.22), apart from the difference

that the upper restriction on ℓ being smaller than $2S$ is absent in the rotor model case. If one is interested primarily in low energy properties, then it appears reasonable to represent each pair of spins by a quantum rotor.

We have seen that the $K/J \to \infty$ limit of H_d closely resembles the $\tilde{g} \to \infty$ limit of H_R. To first order in $\tilde{g}$, we can compare the matrix elements of the term proportional to J in H_R among the low-lying states, with those of the J term in H_d; it is not difficult to see that these matrix elements become equal to each other for an appropriate choice of couplings: see exercise 6.6.1. Therefore we may conclude that the low-energy properties of the two models are closely related for large K/J and $\tilde{g}$. Somewhat different considerations in Chapter 19 will show that the correspondence also applies to the quantum critical point and to the magnetically ordered phase.

The main lesson of the above analysis is that the O(3) quantum rotor model represents the low energy properties of quantum antiferromagnets of Heisenberg spins, with each rotor being an effective representation of a *pair* of antiferromagnetically coupled spins. The strong-coupling spectra clearly indicate the operator correspondence $\hat{\mathbf{L}}_i = \hat{\mathbf{S}}_{1i} + \hat{\mathbf{S}}_{2i}$, and so the rotor angular momentum represents the total angular momentum of the underlying spin system. Examination of matrix elements in the large-S limit shows that $\hat{\mathbf{n}}_i \propto \hat{\mathbf{S}}_{1i} - \hat{\mathbf{S}}_{2i}$: the rotor coordinate $\hat{\mathbf{n}}_i$ is the antiferromagnetic order parameter of the spin system. Magnetically ordered states of the rotor model with $\langle \hat{\mathbf{n}}_i \rangle \neq 0$, which we will encounter below, are therefore spin states with long-range antiferromagnetic order and have a vanishing total ferromagnetic moment. Quantum Heisenberg spin systems with a net ferromagnetic moment are *not* modeled by the quantum rotor model (11.1) – these will be studied in Section 19.2 by a different approach.

Description using Landau-Ginzburg field theory

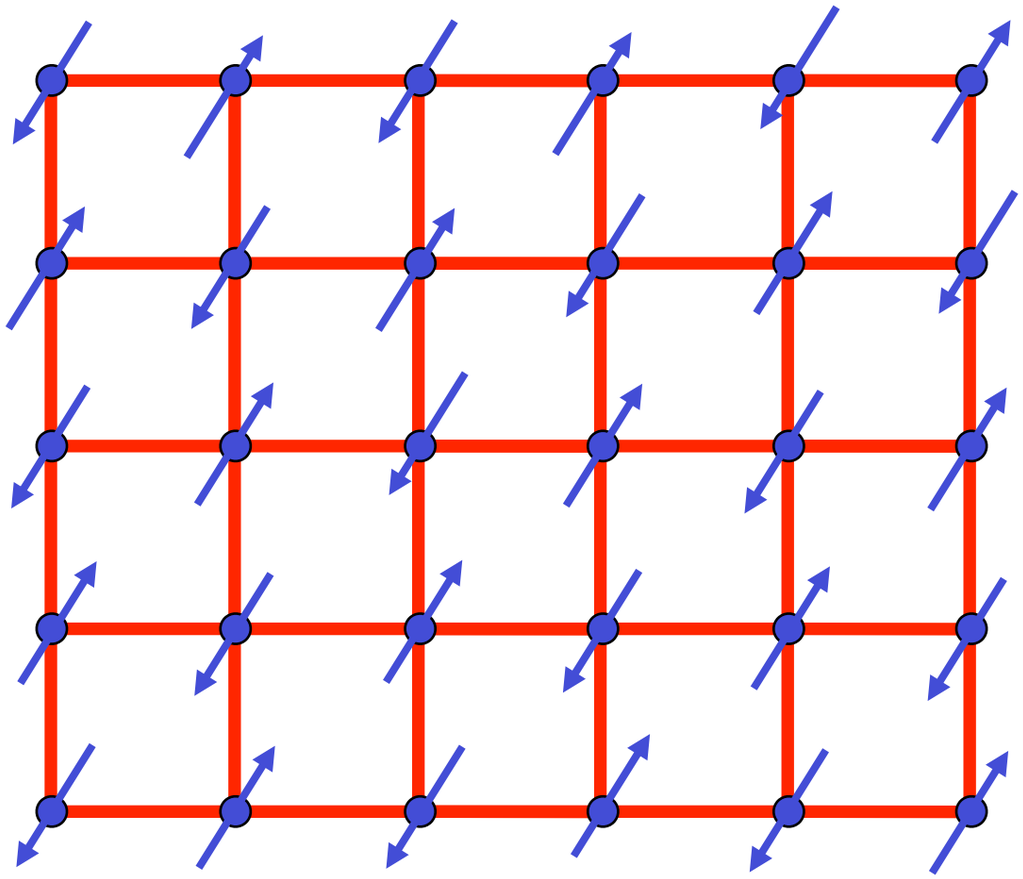

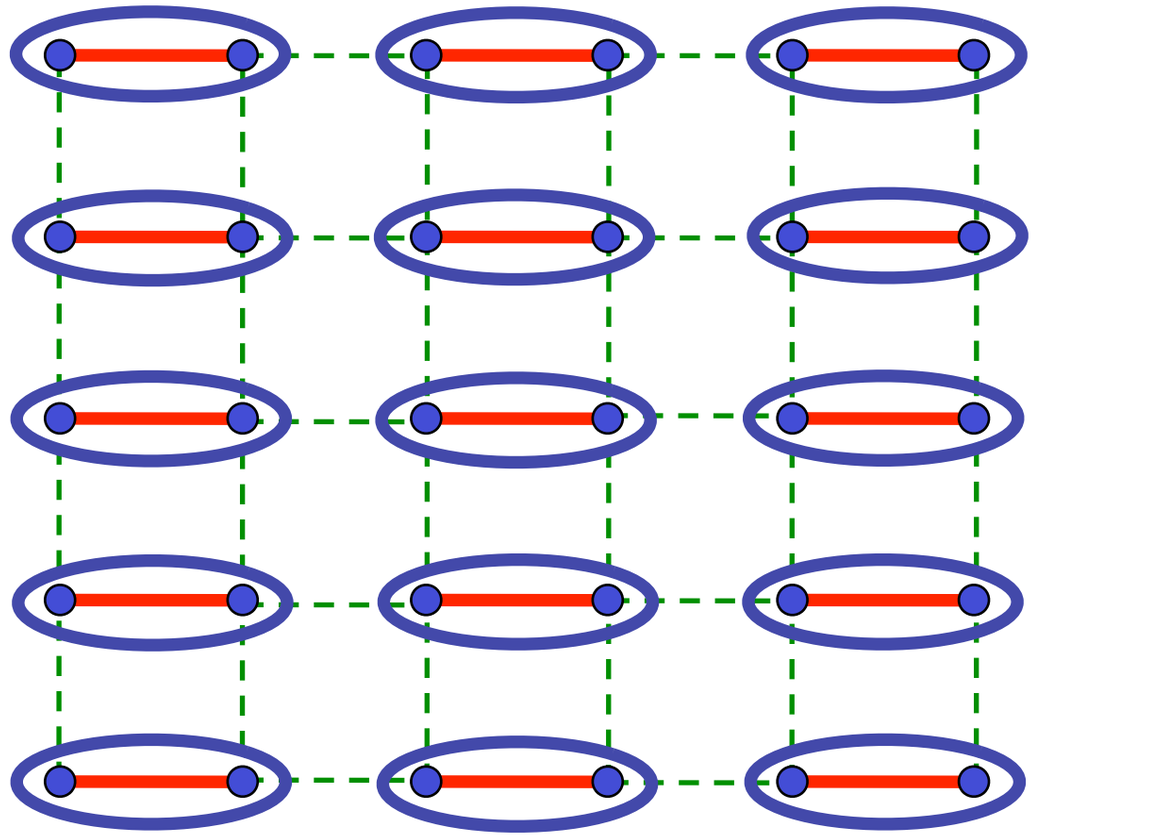

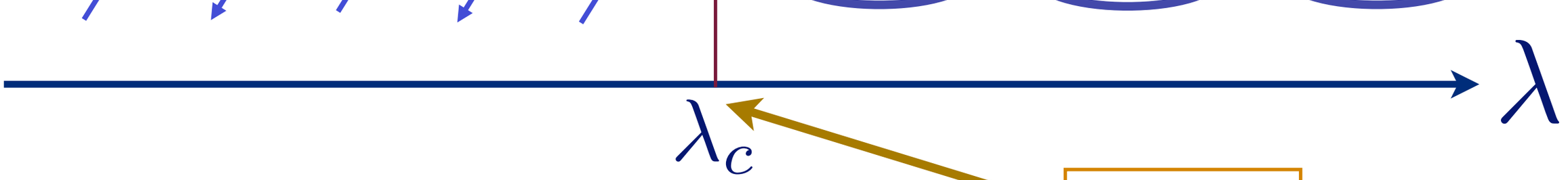

O(3) order parameter $\vec{\varphi}$

$$\mathcal{S} = \int d^2 r d\tau \left[(\partial_\tau \varphi)^2 + c^2 (\nabla_r \vec{\varphi})^2 + (\lambda - \lambda_c) \vec{\varphi}^2 + u \left(\vec{\varphi}^2 \right)^2 \right]$$

Excitation spectrum in the paramagnetic phase

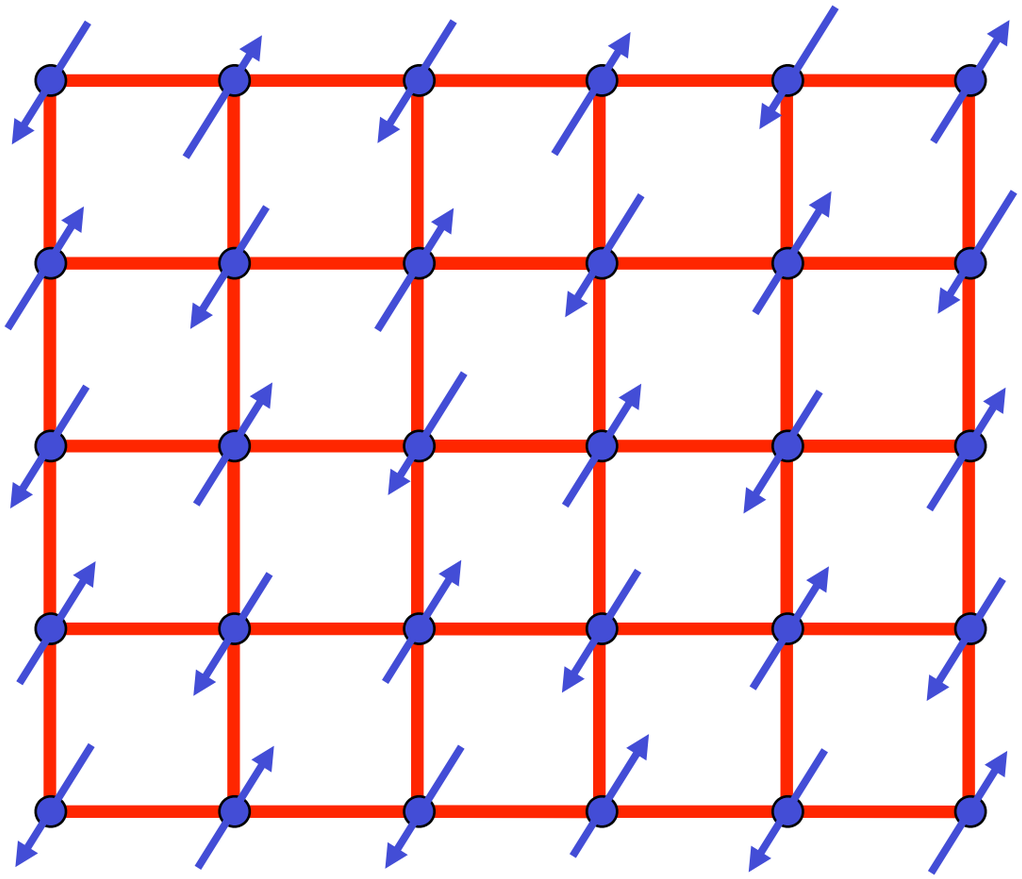

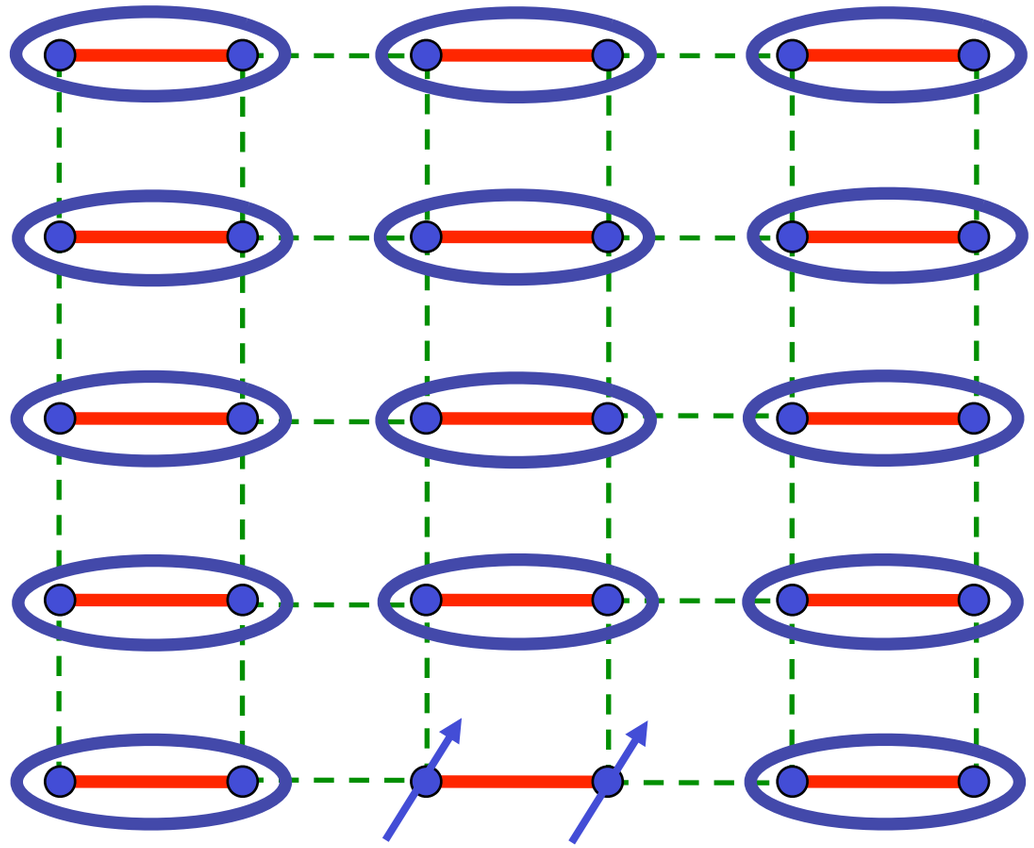

λ

λ_c

$$V(\vec{\varphi}) = (\lambda - \lambda_c)\vec{\varphi}^2 + u\left(\vec{\varphi}^2\right)^2$$

$$\lambda > \lambda_c$$

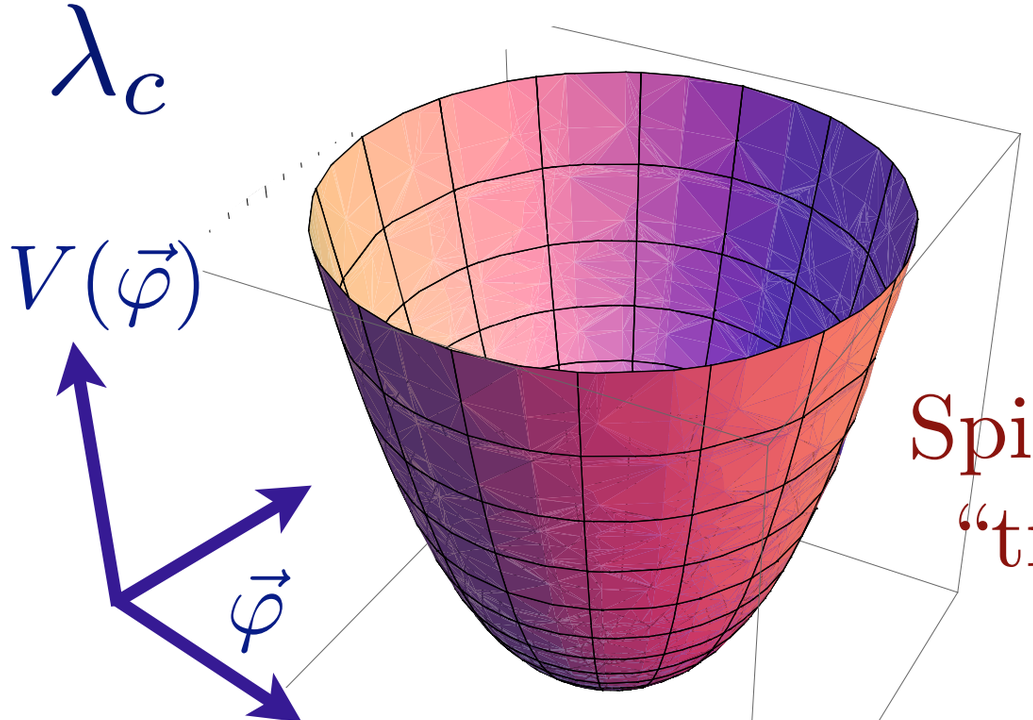

Spin $S = 1$
"triplon"

Excitation spectrum in the paramagnetic phase

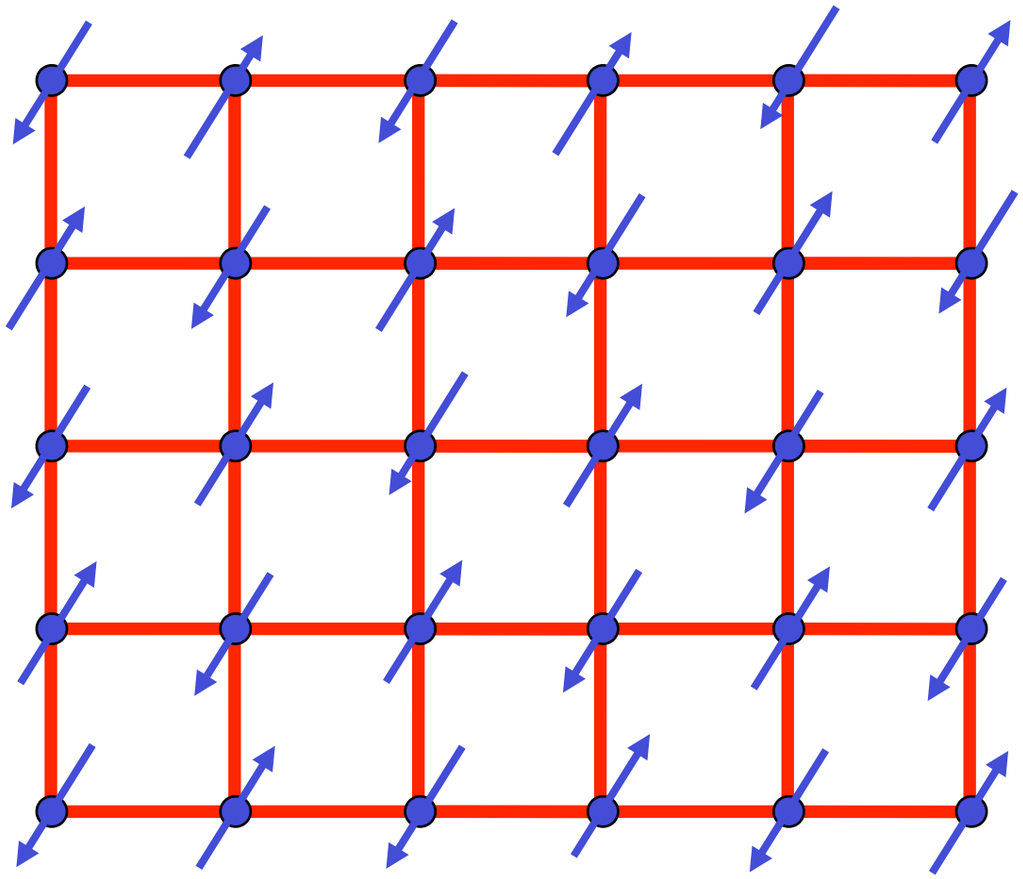

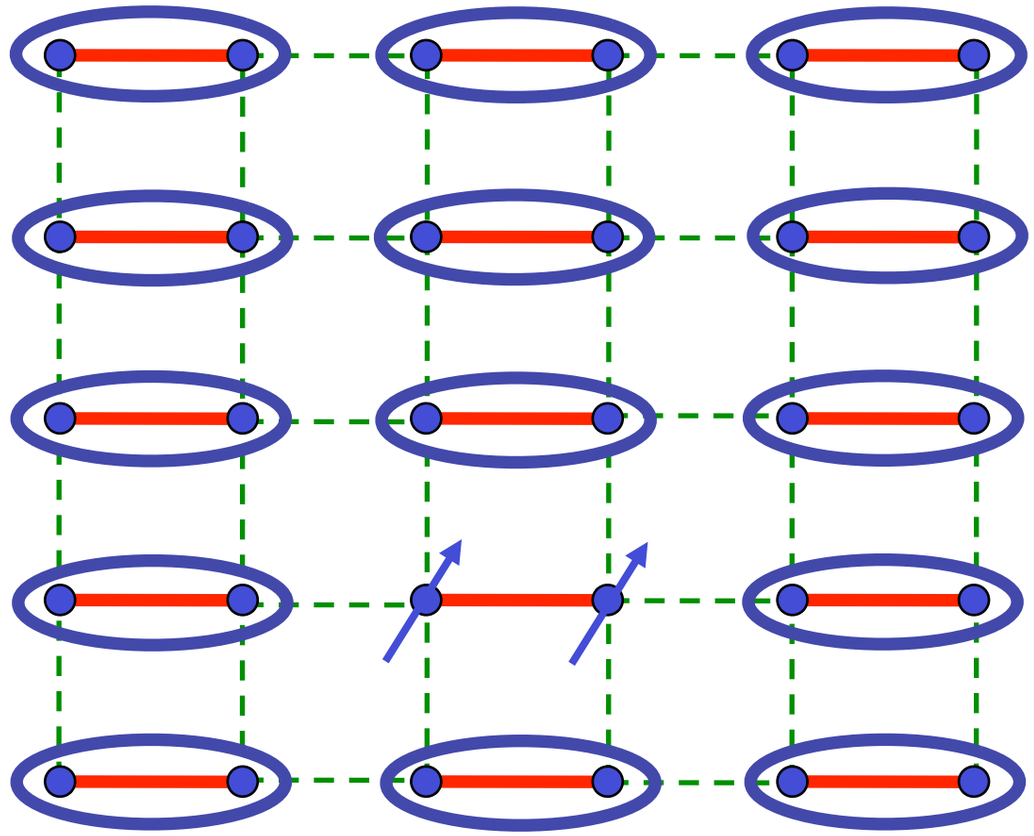

λ

λ_c

$$V(\vec{\varphi}) = (\lambda - \lambda_c)\vec{\varphi}^2 + u\left(\vec{\varphi}^2\right)^2$$

$$\lambda > \lambda_c$$

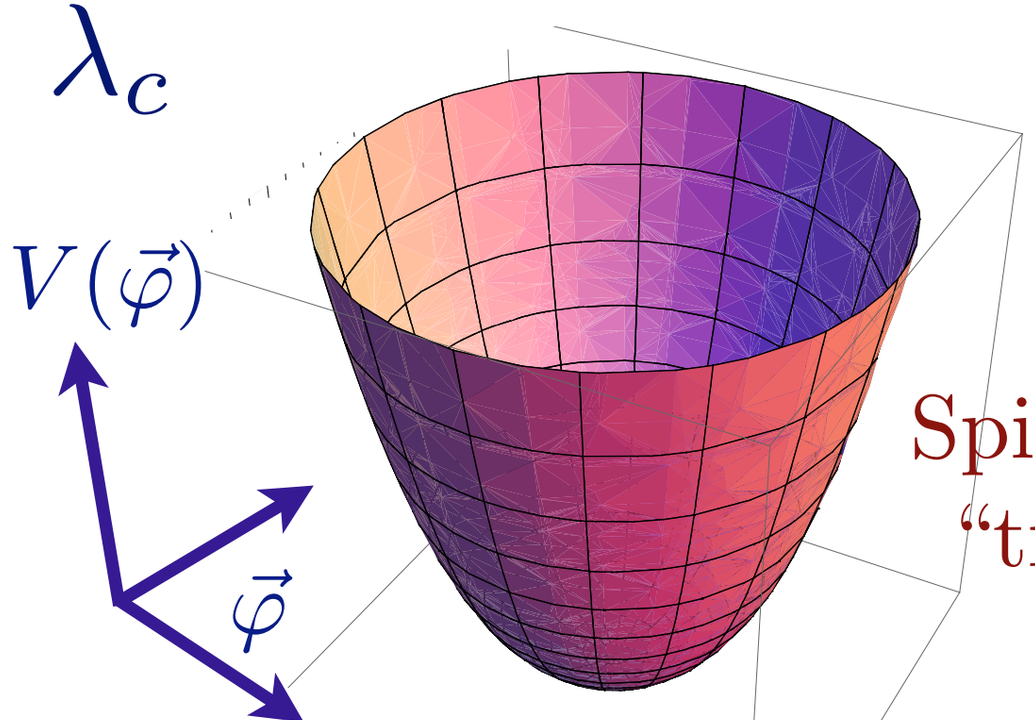

Spin $S = 1$
"triplon"

Excitation spectrum in the paramagnetic phase

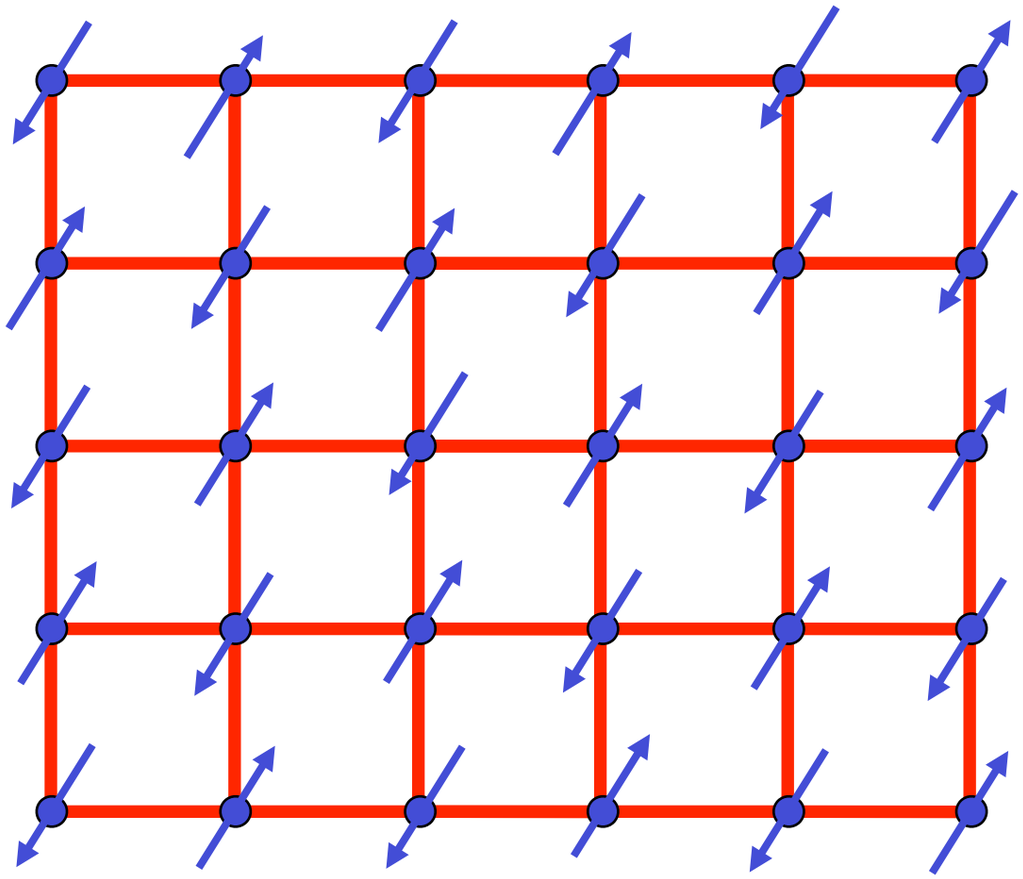

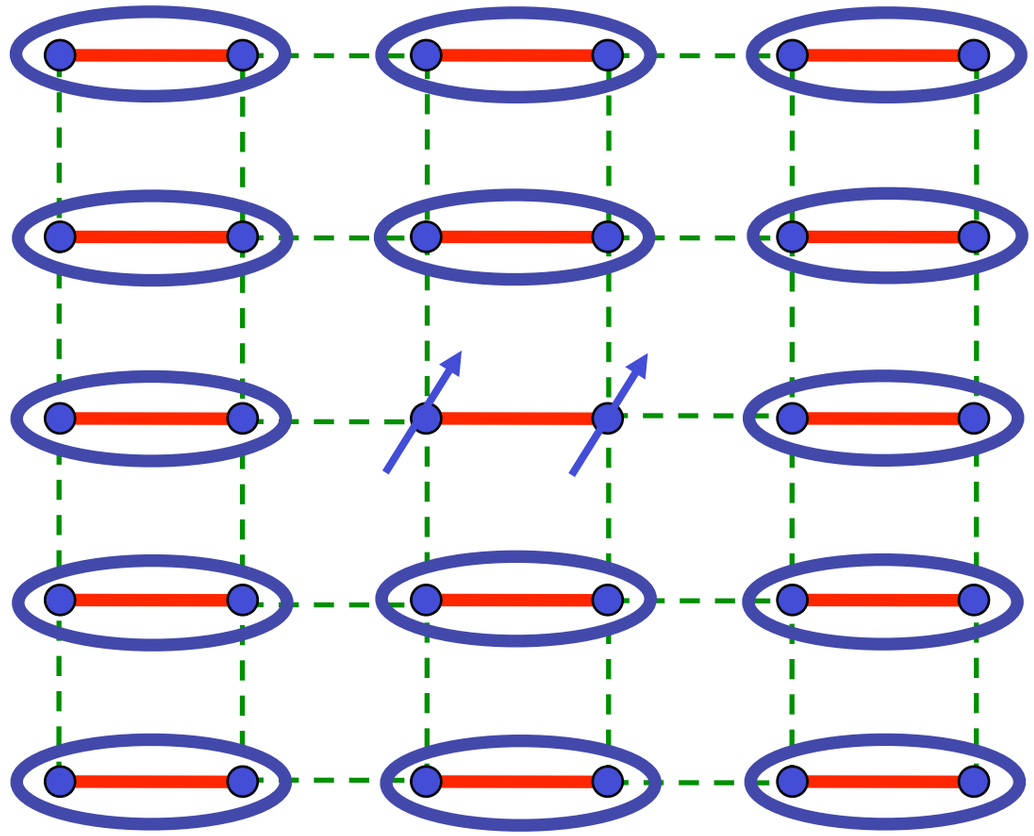

λ

λ_c

$$V(\vec{\varphi}) = (\lambda - \lambda_c)\vec{\varphi}^2 + u\left(\vec{\varphi}^2\right)^2$$

$$\lambda > \lambda_c$$

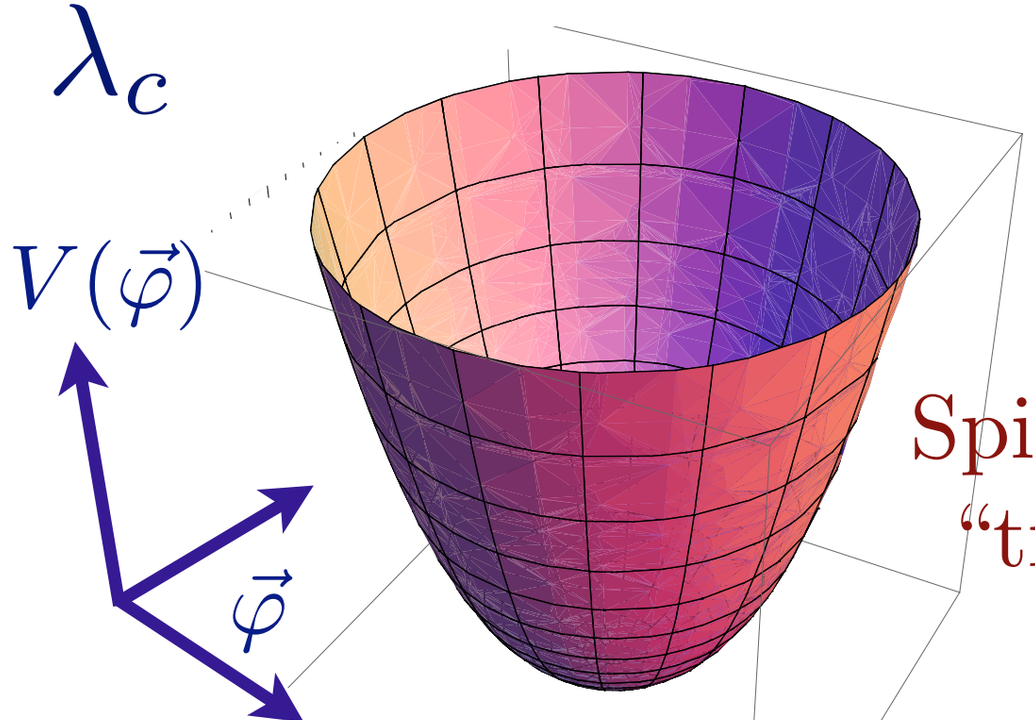

Spin $S = 1$
"triplon"

Excitation spectrum in the paramagnetic phase

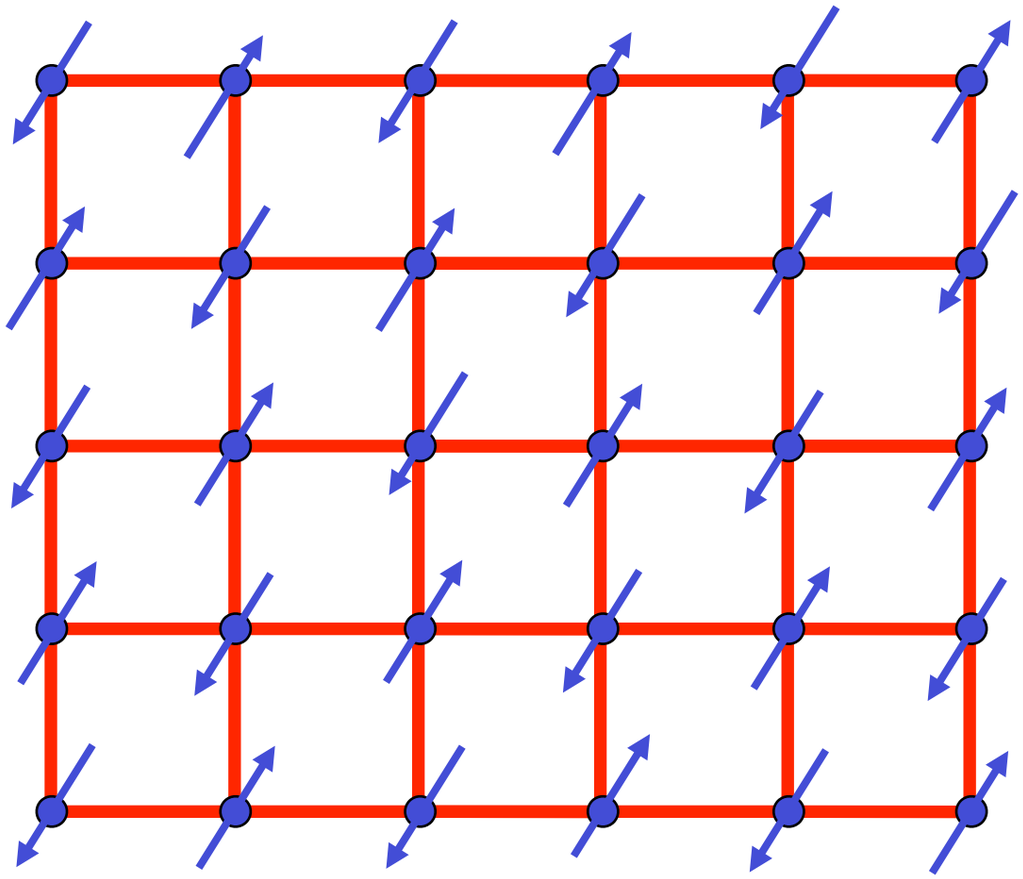

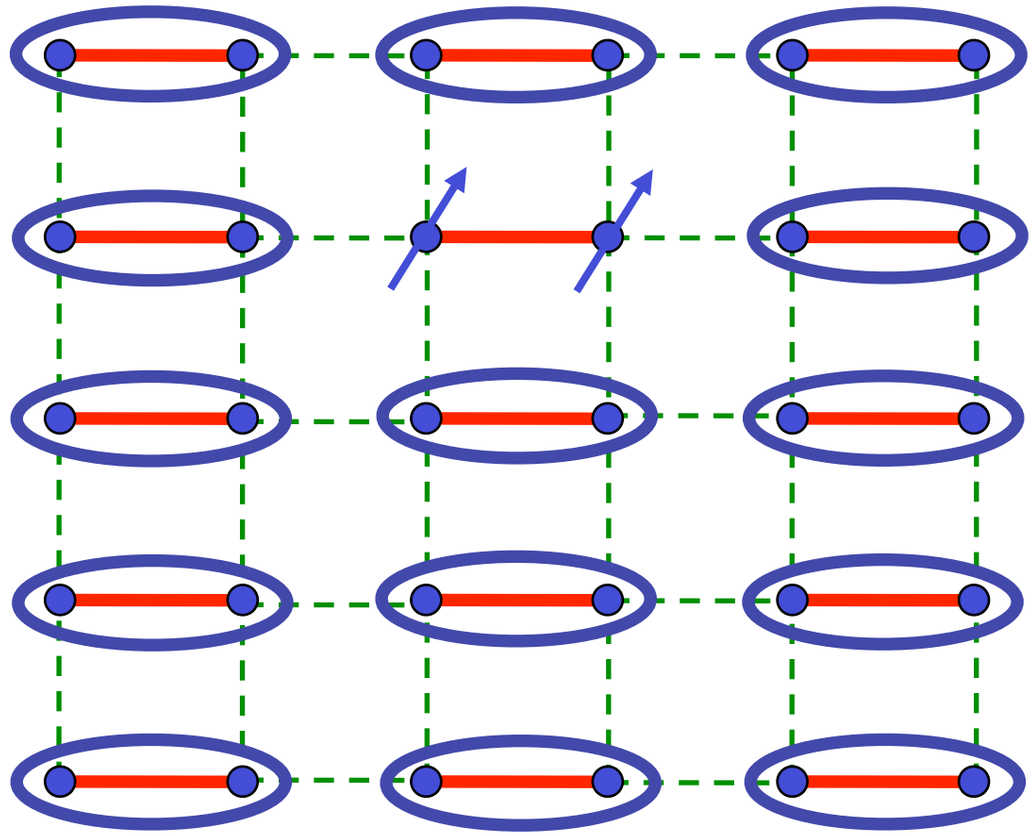

λ

λ_c

$$V(\vec{\varphi}) = (\lambda - \lambda_c)\vec{\varphi}^2 + u\left(\vec{\varphi}^2\right)^2$$

$$\lambda > \lambda_c$$

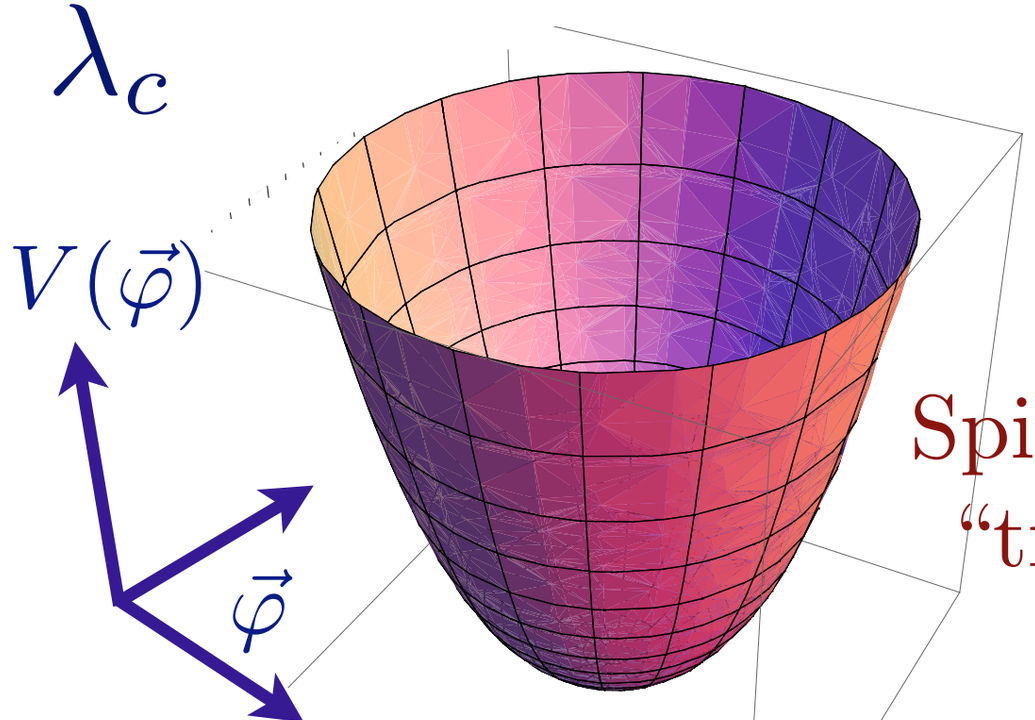

Spin $S = 1$
"triplon"

Excitation spectrum in the paramagnetic phase

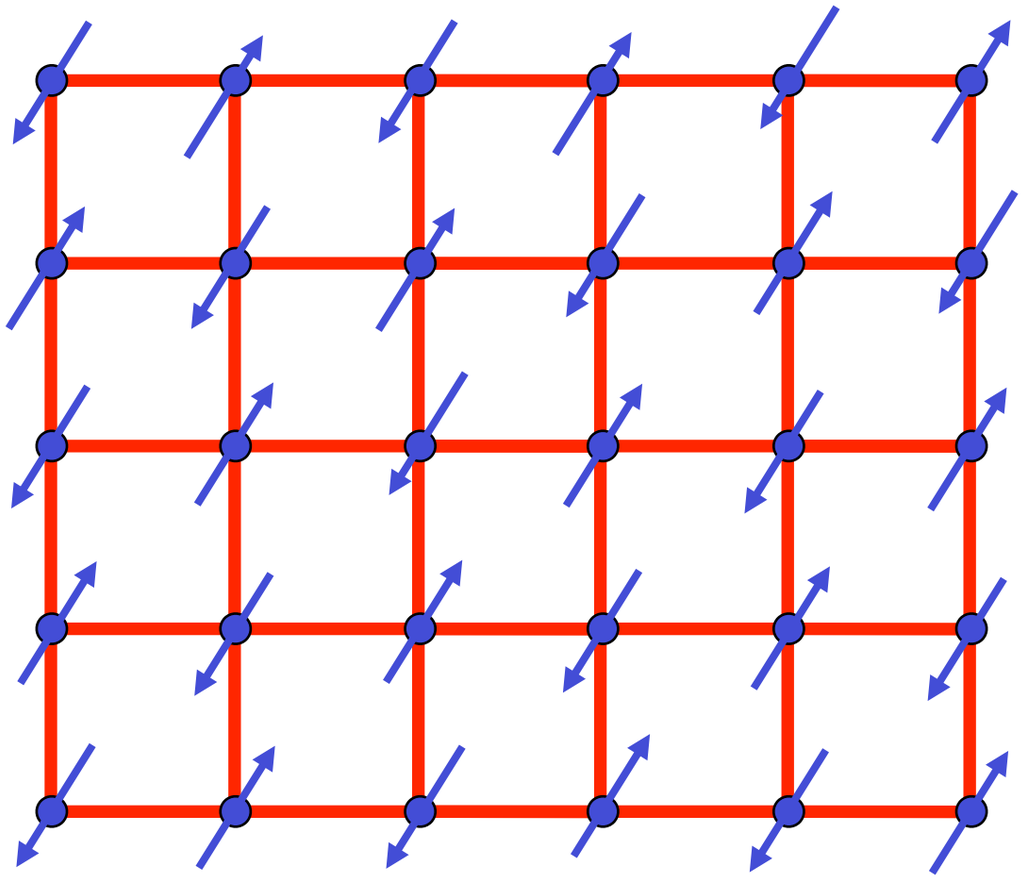

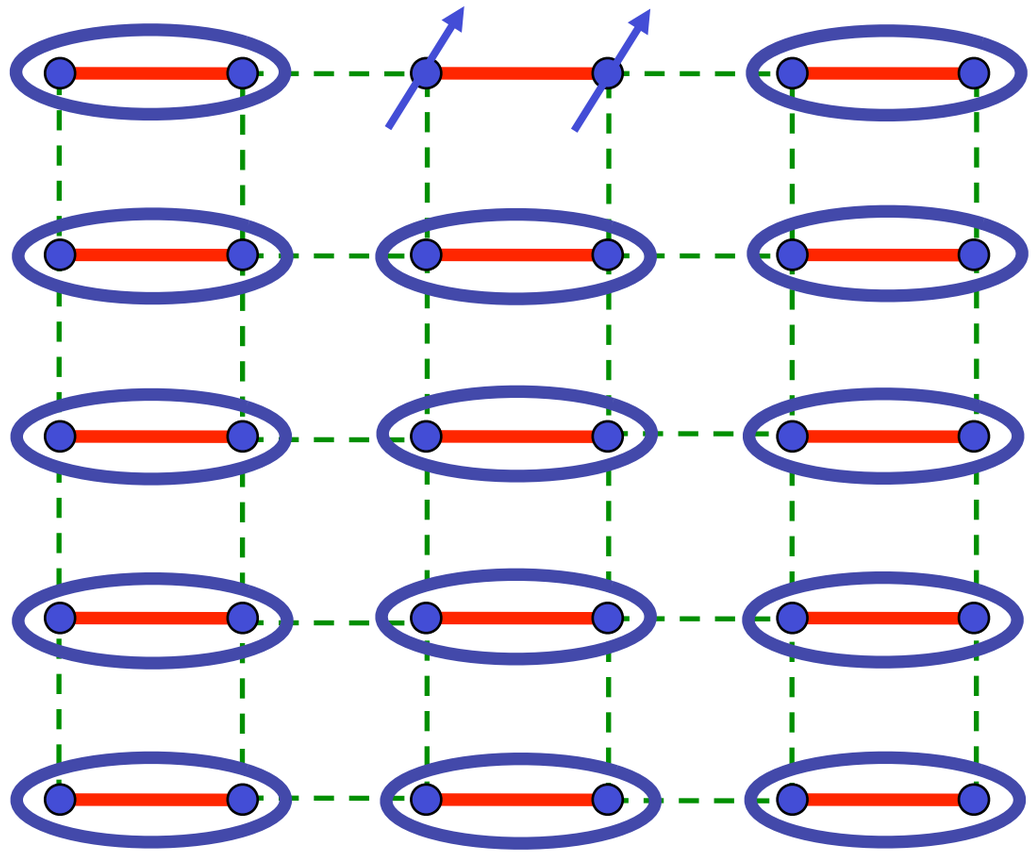

λ

λ_c

$$V(\vec{\varphi}) = (\lambda - \lambda_c)\vec{\varphi}^2 + u\left(\vec{\varphi}^2\right)^2$$

$$\lambda > \lambda_c$$

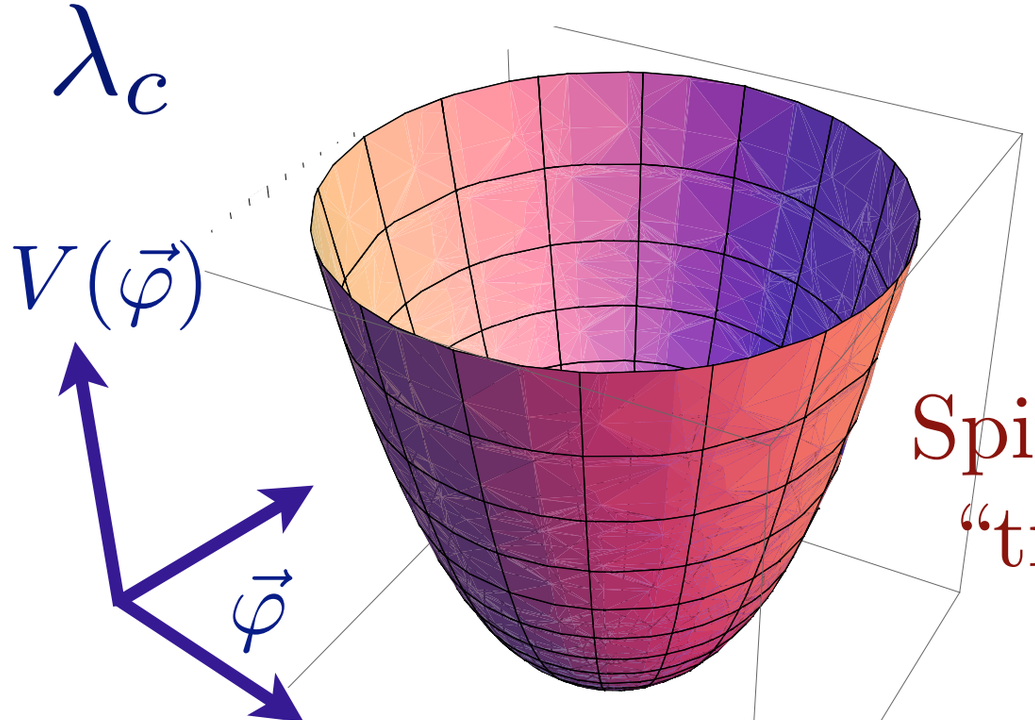

Spin $S = 1$
"triplon"

Excitation spectrum in the Néel phase

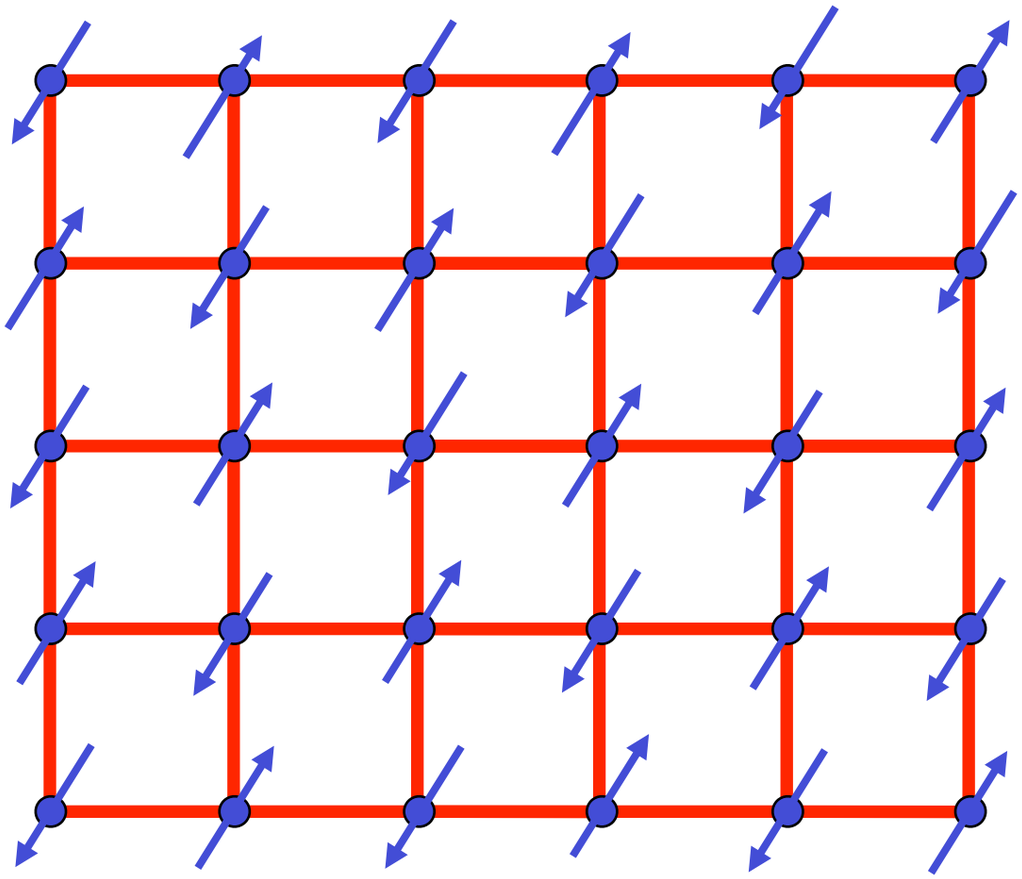

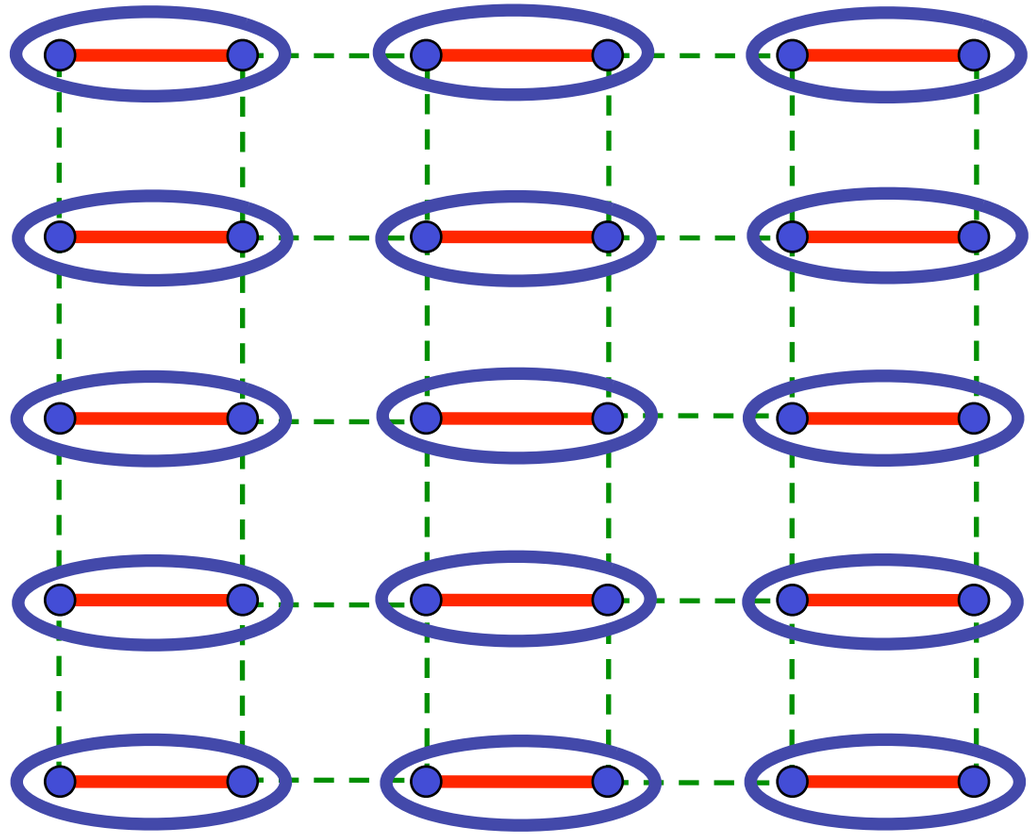

λ

λ_c

$$V(\vec{\varphi}) = (\lambda - \lambda_c)\vec{\varphi}^2 + u\left(\vec{\varphi}^2\right)^2$$

$$\lambda < \lambda_c$$

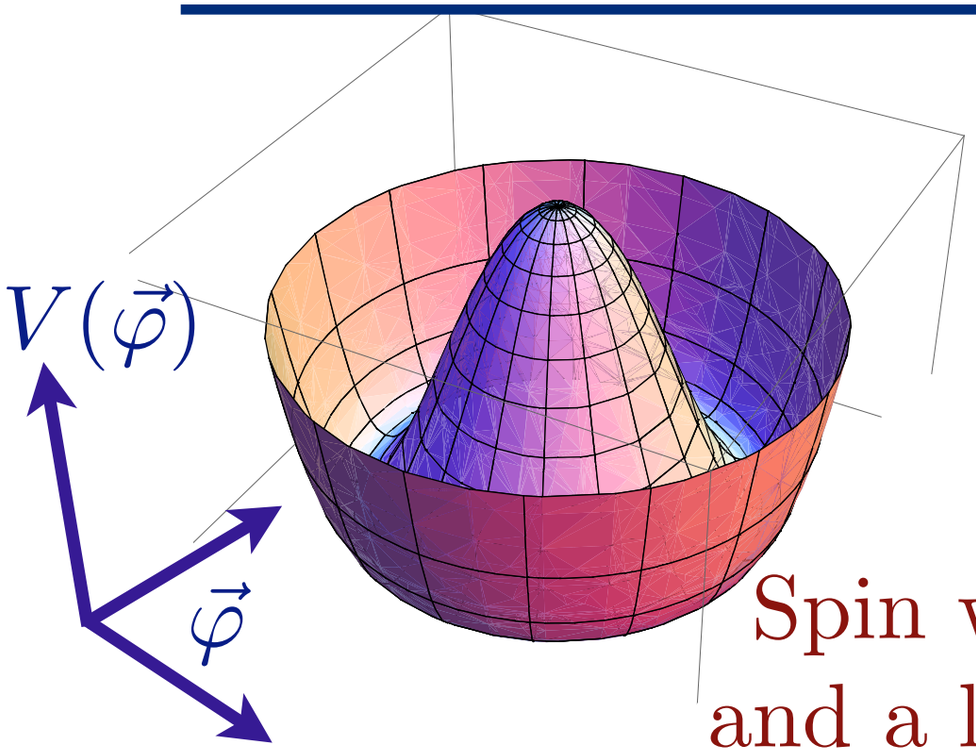

Spin waves ("Goldstone" modes)
and a longitudinal "Higgs" particle

Excitation spectrum in the Néel phase

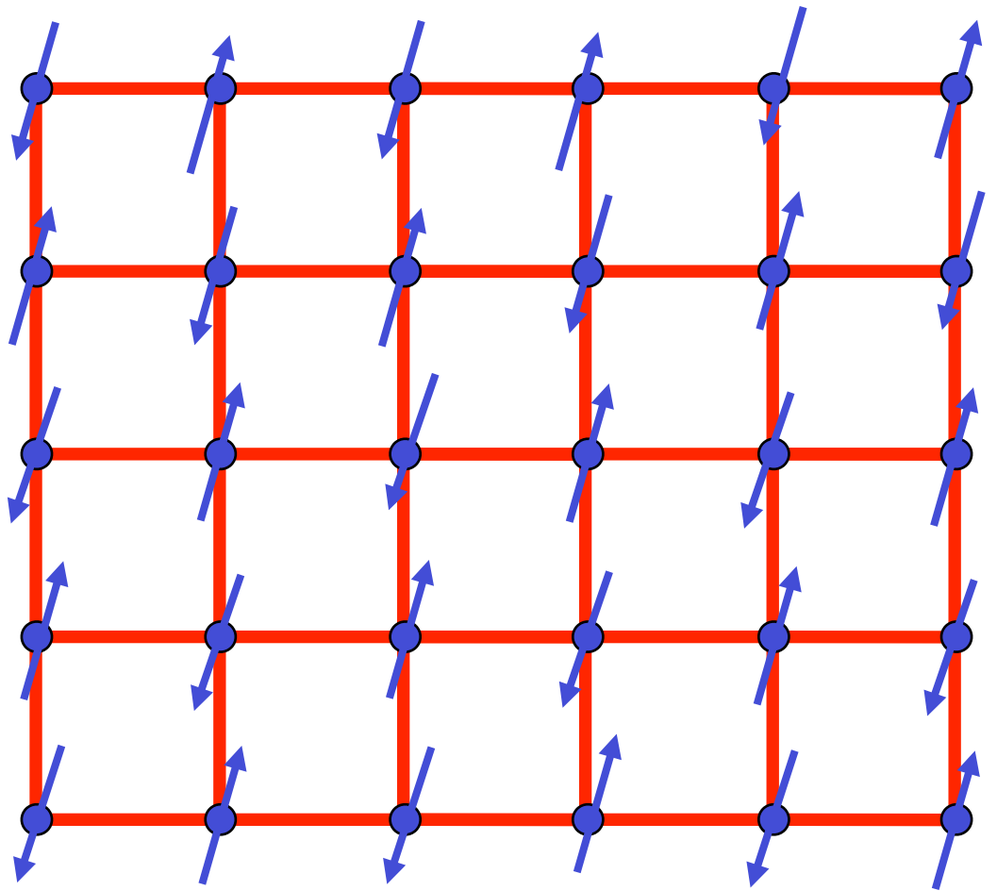

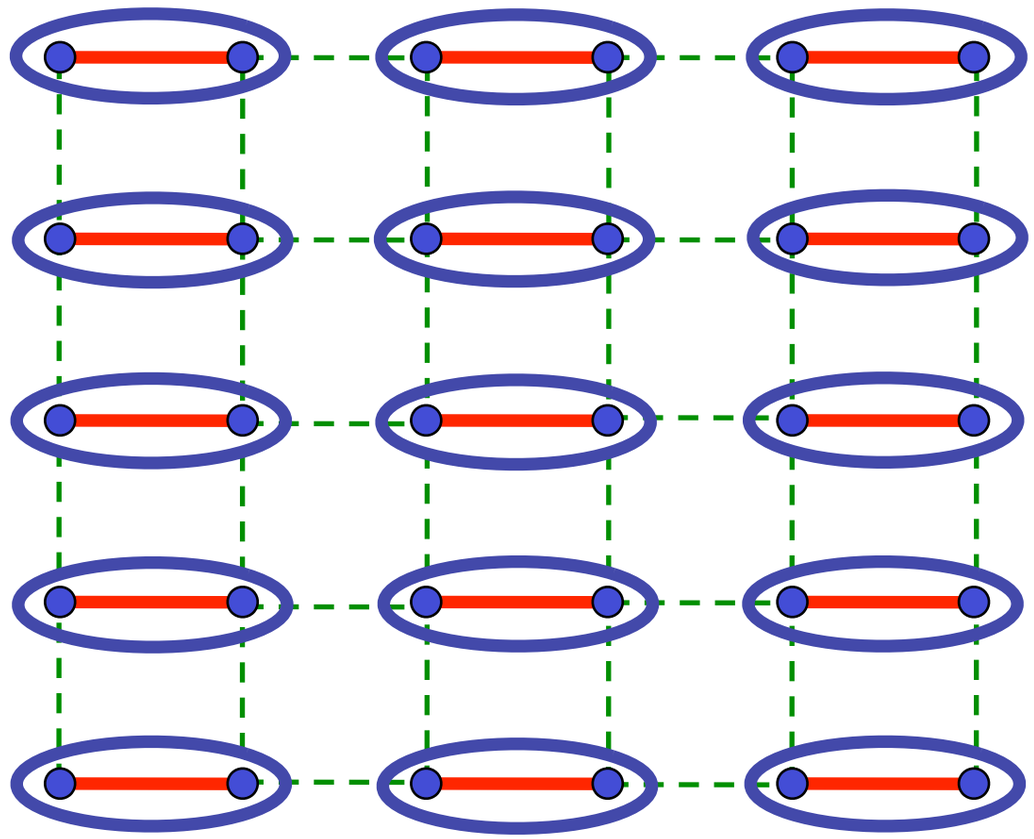

λ

λ_c

$$V(\vec{\varphi}) = (\lambda - \lambda_c)\vec{\varphi}^2 + u\left(\vec{\varphi}^2\right)^2$$

$$\lambda < \lambda_c$$

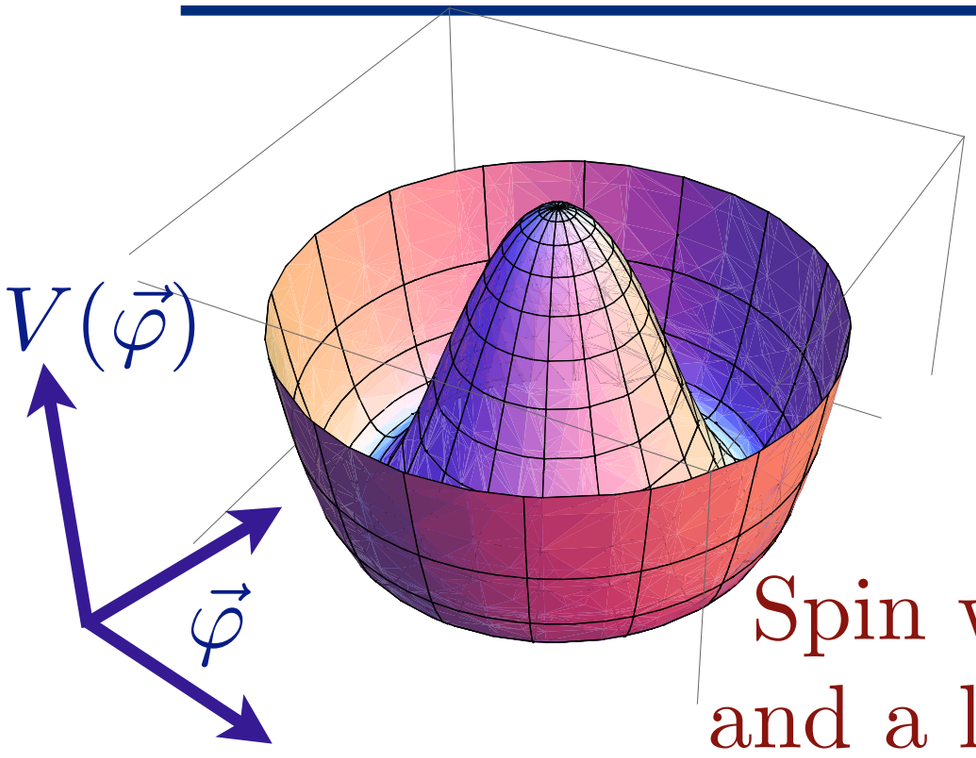

Spin waves ("Goldstone" modes)
and a longitudinal "Higgs" particle

Excitation spectrum in the Néel phase

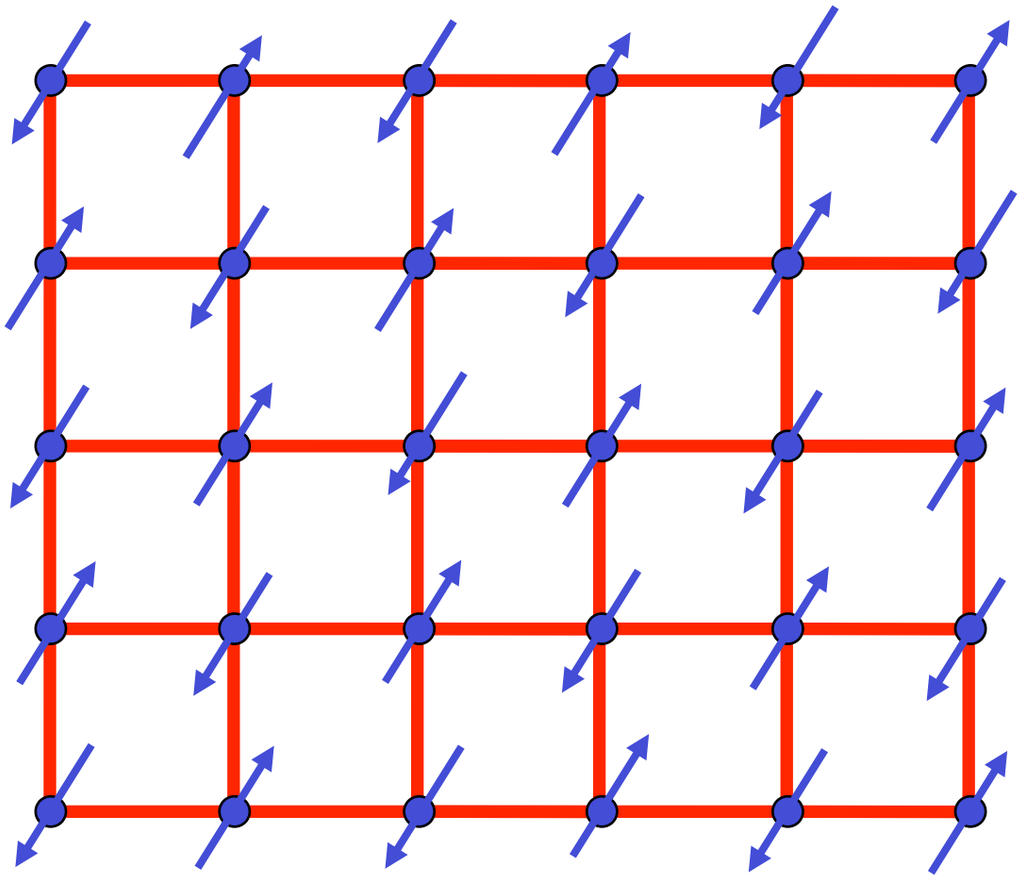

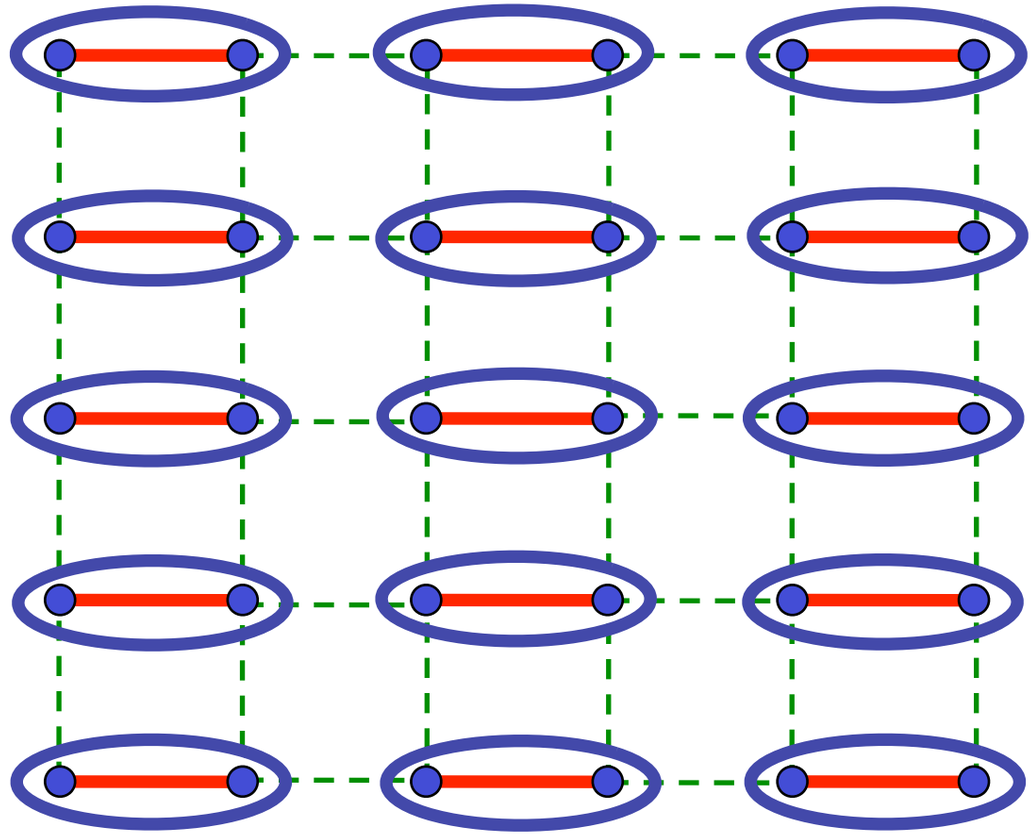

λ

λ_c

$$V(\vec{\varphi}) = (\lambda - \lambda_c)\vec{\varphi}^2 + u\left(\vec{\varphi}^2\right)^2$$

$$\lambda < \lambda_c$$

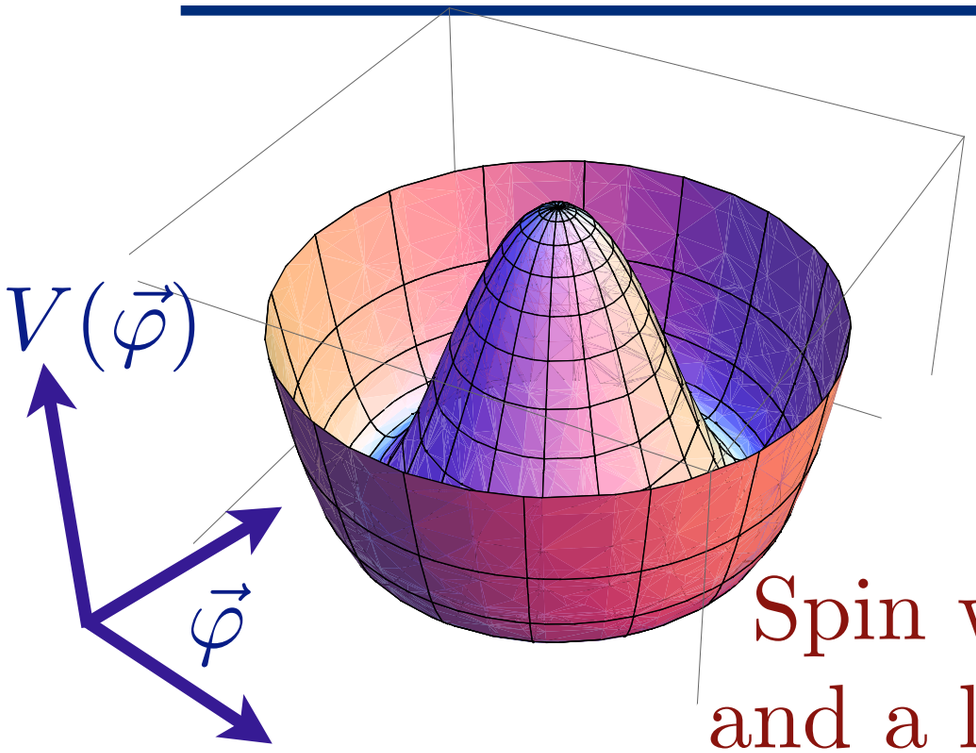

Spin waves ("Goldstone" modes)
and a longitudinal "Higgs" particle

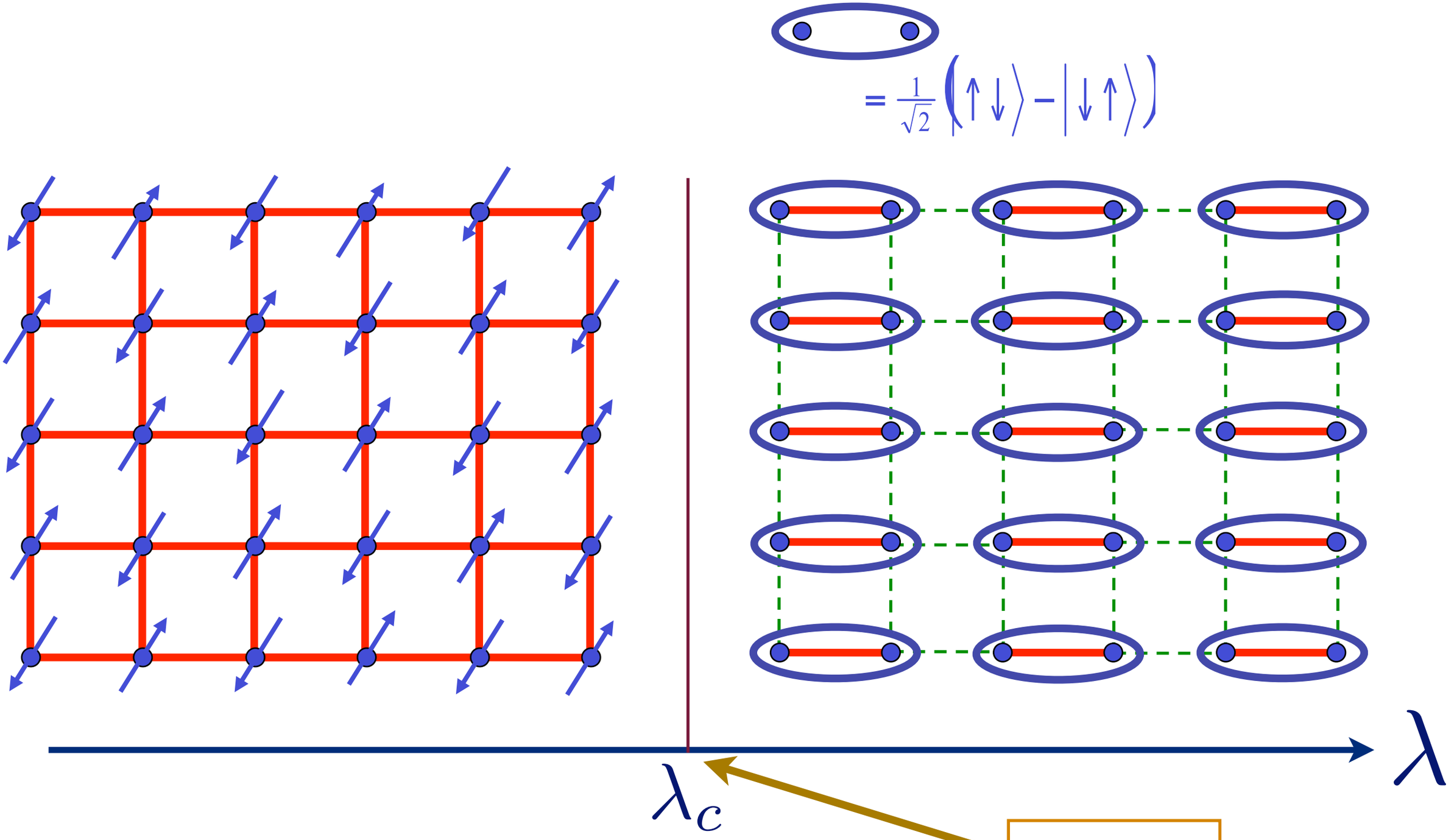

O(3) order parameter $\vec{\varphi}$

$$\mathcal{S} = \int d^2 r d\tau \left[(\partial_\tau \varphi)^2 + c^2 (\nabla_r \vec{\varphi})^2 + s\vec{\varphi}^2 + u\left(\vec{\varphi}^2\right)^2 \right]$$

Quantum Monte Carlo - critical exponents

Table IV: Fit results for the critical exponents ν, β/ν, and η. We summarize results including a variation of the critical point within its error bar. For the ladder model (top group of values) fit results and quality of fits are also given at the previous best estimate of α_c. The bottom group are results for the plaquette model. Numbers in [. . .] brackets denote the χ^2/d.o.f. For comparison relevant reference values for the 3D $O(3)$ universality class are given in the last line.

α_c	ν^a	β/ν^b	η^c
$1.9096 - \sigma$	0.712(4) [1.8]	0.516(2) [0.5]	0.026(2) [0.2]
1.9096	0.711(4) [1.8]	0.518(2) [1.1]	0.029(5) [0.8]
$1.9096 + \sigma$	0.710(4) [1.8]	0.519(3) [2.5]	0.032(7) [1.4]
1.9107^d	0.709(3) [1.7]	0.525(8) [15.3]	0.051(10) [12]
$1.8230 - \sigma$	0.708(4) [0.99]	0.515(2) [0.84]	0.025(4) [0.15]
1.8230	0.706(4) [1.04]	0.516(2) [0.40]	0.028(3) [0.31]
$1.8230 + \sigma$	0.706(4) [1.10]	0.517(2) [1.6]	0.031(5) [0.80]
Ref. 49	0.7112(5)	0.518(1)	0.0375(5)

[a] $L > 12$.
[b] $L > 16$.
[c] $L > 20$.
[d] Previous best estimate of Ref. 19.

S. Wenzel and W. Janke, *Phys. Rev. B* **79**, 014410 (2009)
M. Troyer, M. Imada, and K. Ueda, *J. Phys. Soc. Japan* (1997)

Quantum Monte Carlo - critical exponents

Table IV: Fit results for the critical exponents ν, β/ν, and η. We summarize results including a variation of the critical point within its error bar. For the ladder model (top group of values) fit results and quality of fits are also given at the previous best estimate of α_c. The bottom group are results for the plaquette model. Numbers in [. . .] brackets denote the χ^2/d.o.f. For comparison relevant reference values for the 3D $O(3)$ universality class are given in the last line.

α_c	ν^a	β/ν^b	η^c
$1.9096 - \sigma$	0.712(4) [1.8]	0.516(2) [0.5]	0.026(2) [0.2]
1.9096	0.711(4) [1.8]	0.518(2) [1.1]	0.029(5) [0.8]
$1.9096 + \sigma$	0.710(4) [1.8]	0.519(3) [2.5]	0.032(7) [1.4]
1.9107^d	0.709(3) [1.7]	0.525(8) [15.3]	0.051(10) [12]
$1.8230 - \sigma$	0.708(4) [0.99]	0.515(2) [0.84]	0.025(4) [0.15]
1.8230	0.706(4) [1.04]	0.516(2) [0.40]	0.028(3) [0.31]
$1.8230 + \sigma$	0.706(4) [1.10]	0.517(2) [1.6]	0.031(5) [0.80]
Ref. 49	0.7112(5)	0.518(1)	0.0375(5)

[a] $L > 12$.
[b] $L > 16$.
[c] $L > 20$.
[d] Previous best estimate of Ref. 19.

Field-theoretic RG of CFT3 E. Vicari *et al.*

S. Wenzel and W. Janke, *Phys. Rev. B* **79**, 014410 (2009)
M. Troyer, M. Imada, and K. Ueda, *J. Phys. Soc. Japan* (1997)

$TlCuCl_3$

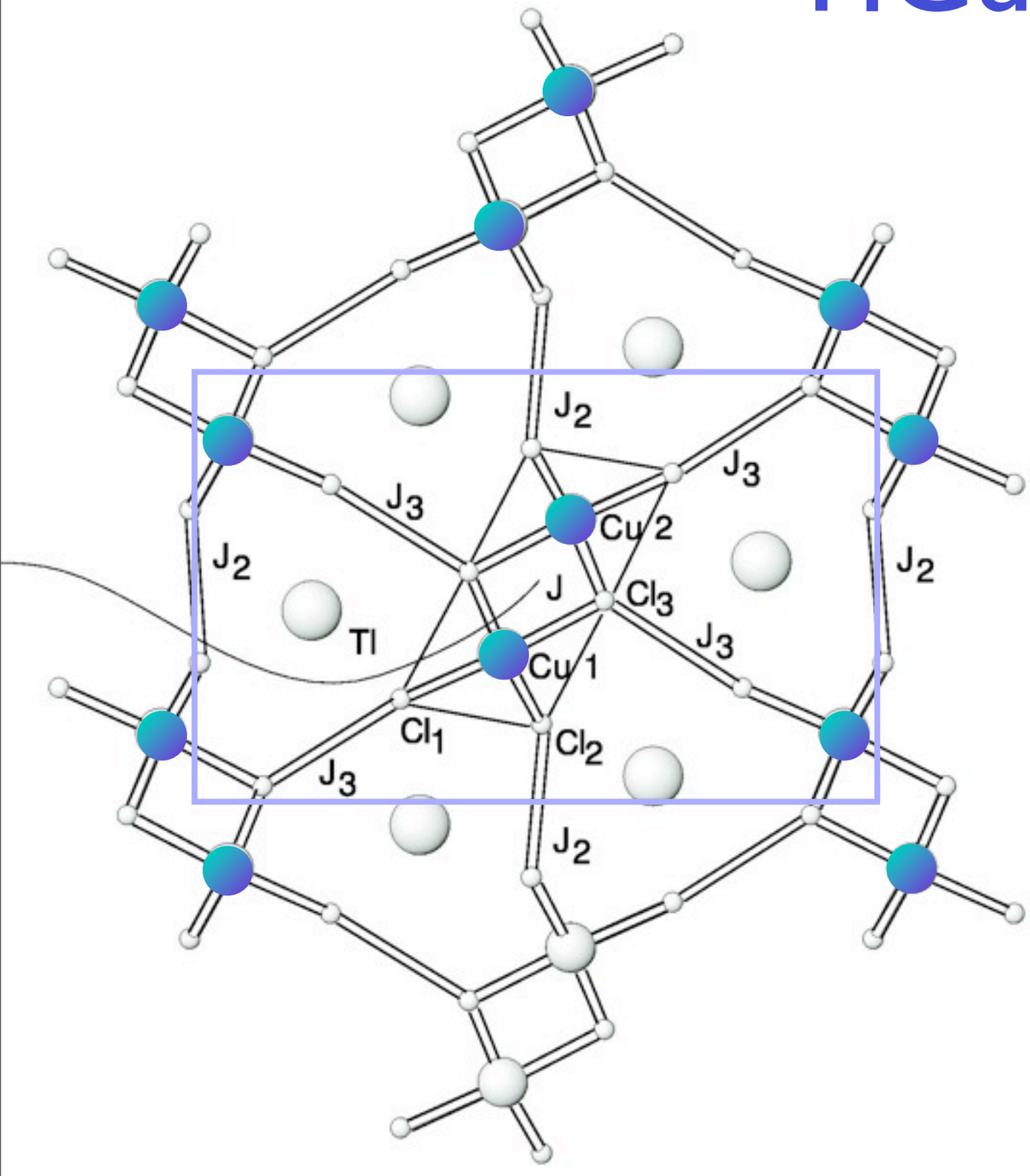
J2
J3
J3
J2
Cu2
J
Cl3
J2
Tl
J3
Cu1
Cl1
Cl2
J3
J2

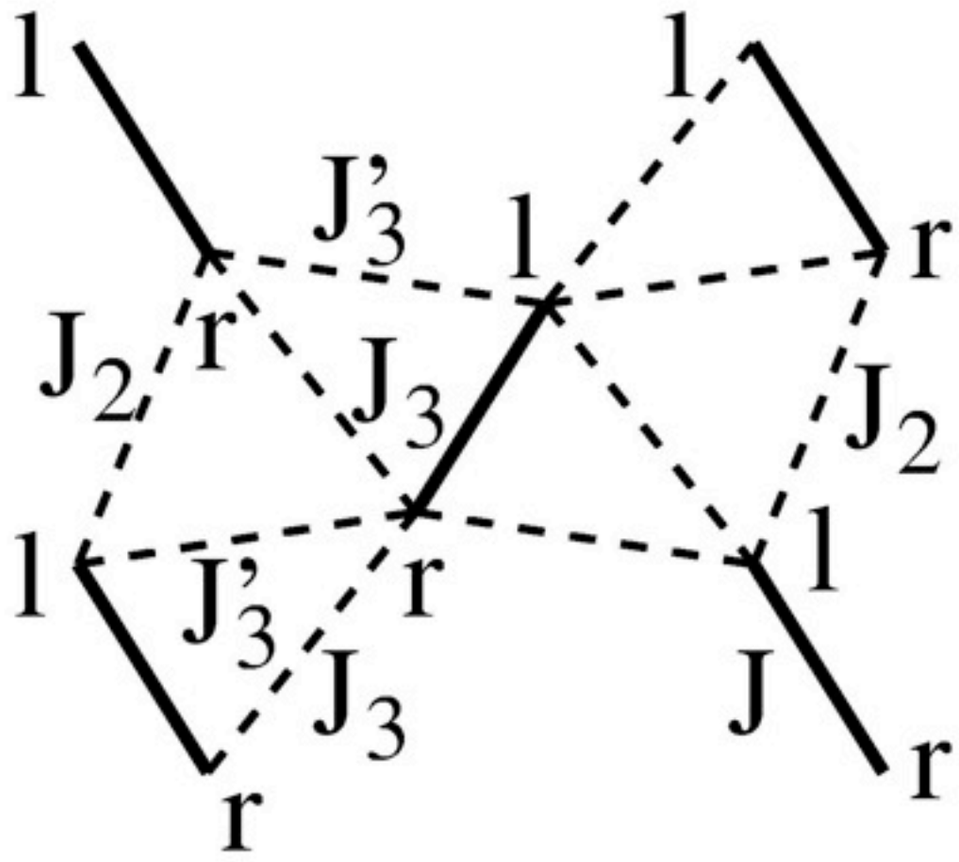
l
J'3
l
r
J2
r
J3
J2
l
J'3
r
l
J3
J
r
r

$TlCuCl_3$

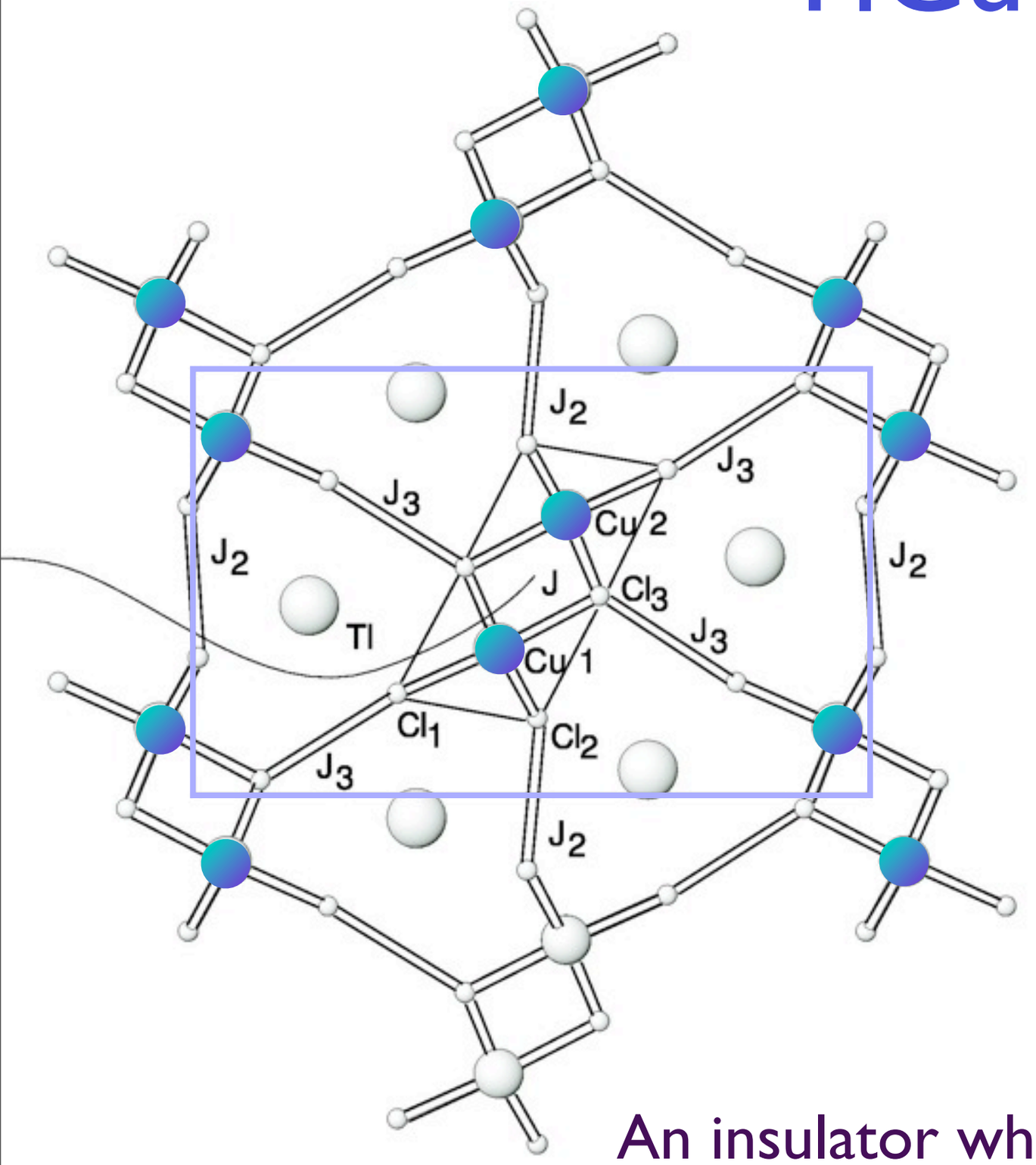

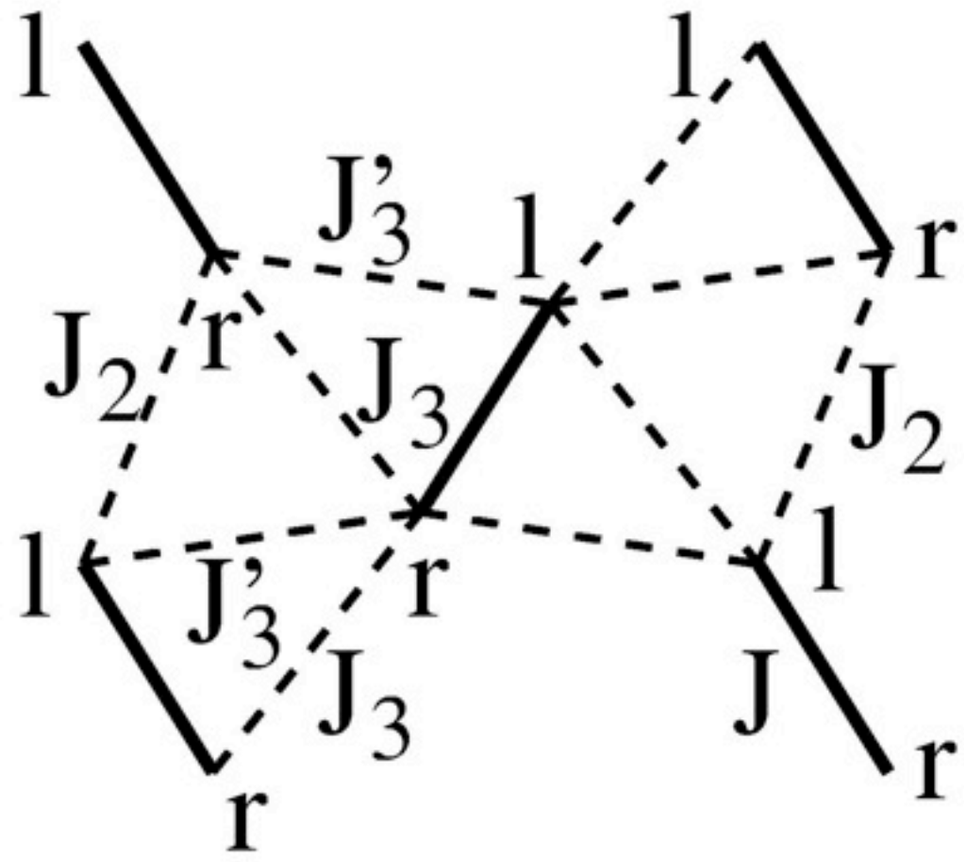

An insulator whose spin susceptibility vanishes exponentially as the temperature T tends to zero.

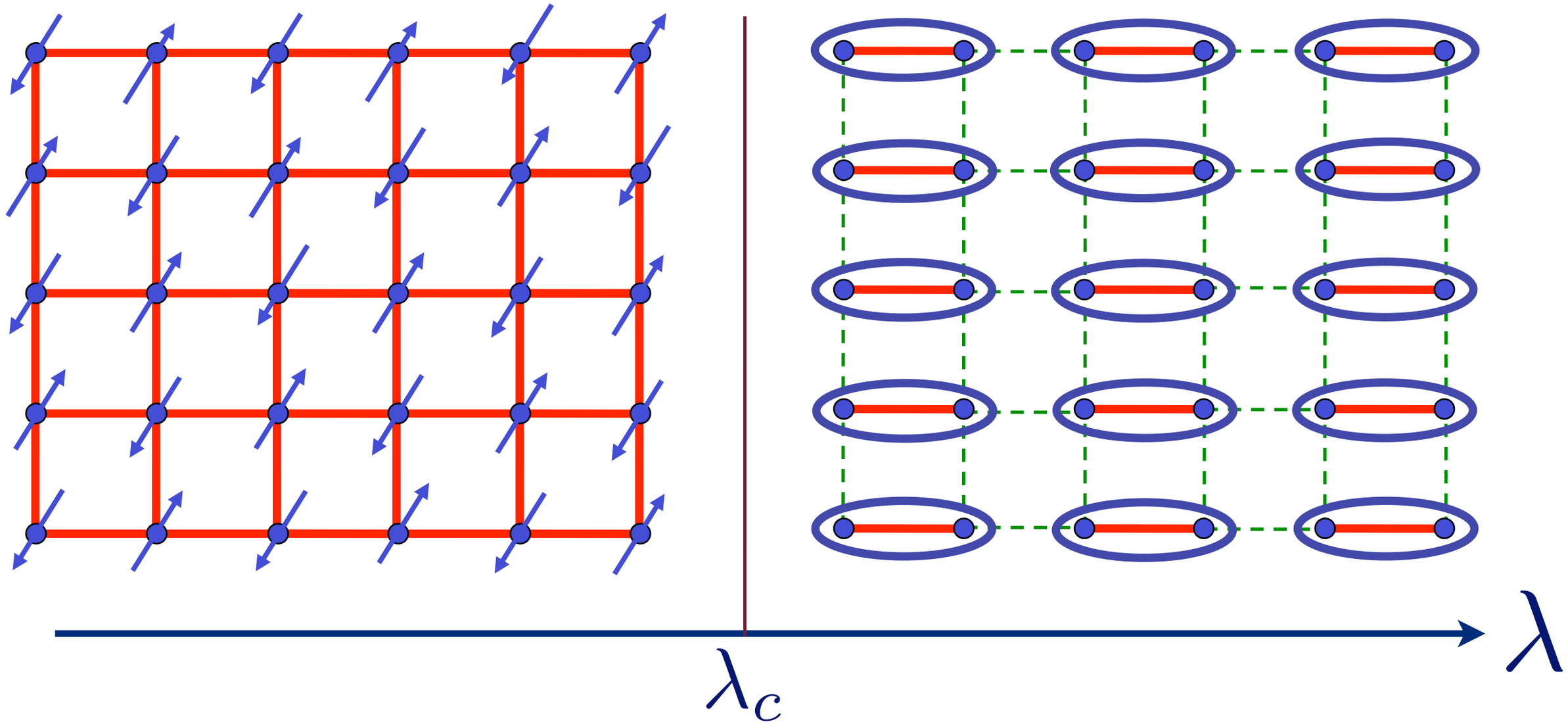

Pressure in $TlCuCl_3$

$TlCuCl_3$ at ambient pressure

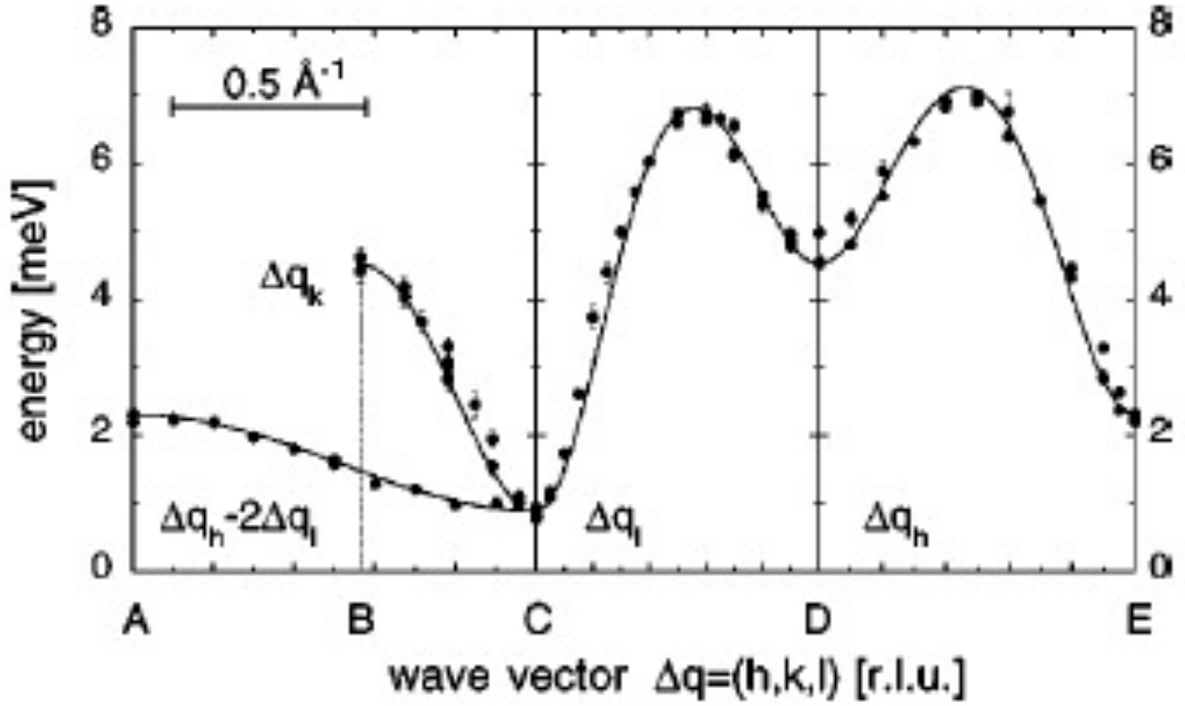

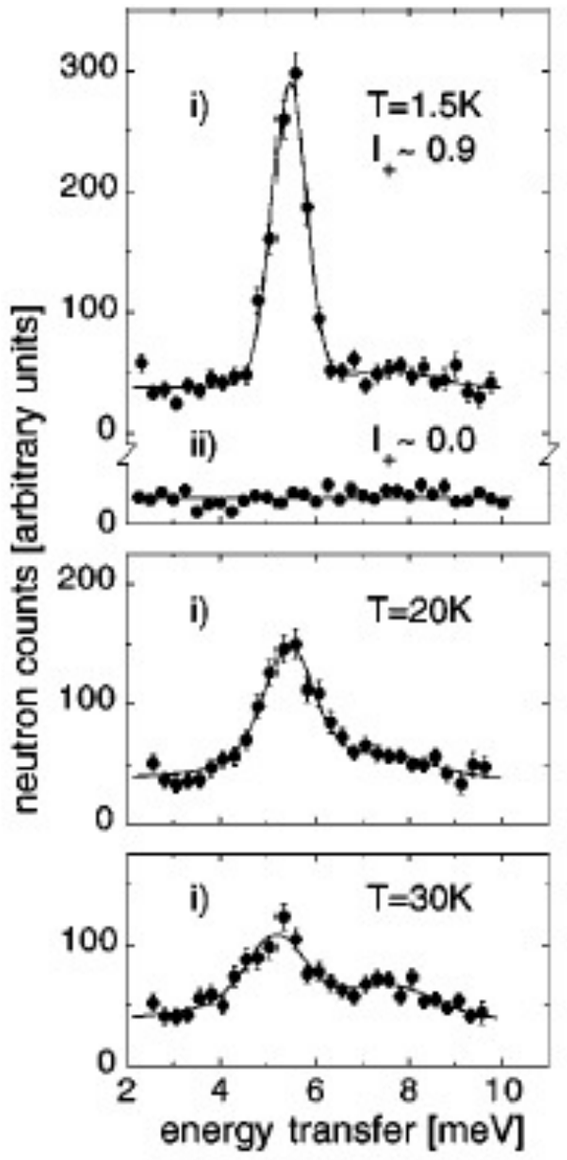

FIG. 1. Measured neutron profiles in the a^*c^* plane of $TlCuCl_3$ for $i=(1.35,0,0)$, $ii=(0,0,3.15)$ [r.l.u]. The spectrum at $T=1.5$ K

N. Cavadini, G. Heigold, W. Henggeler, A. Furrer, H.-U. Güdel, K. Krämer and H. Mutka, *Phys. Rev.* B 63 172414 (2001).

$TlCuCl_3$ at ambient pressure

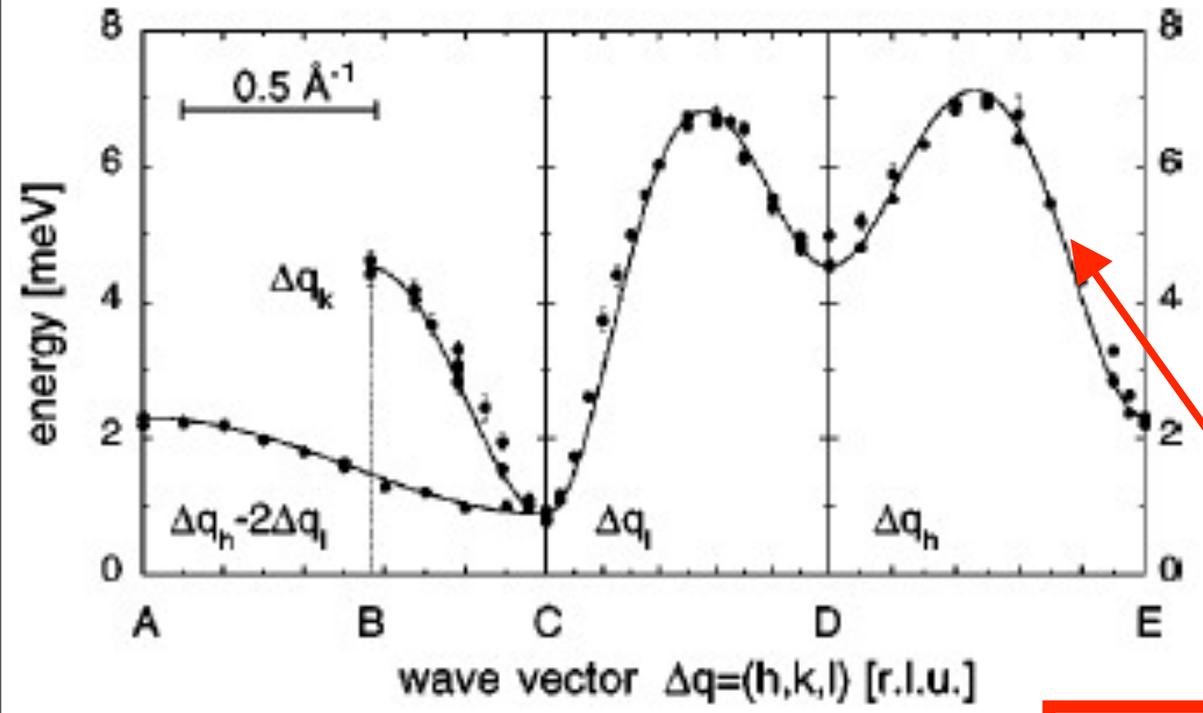

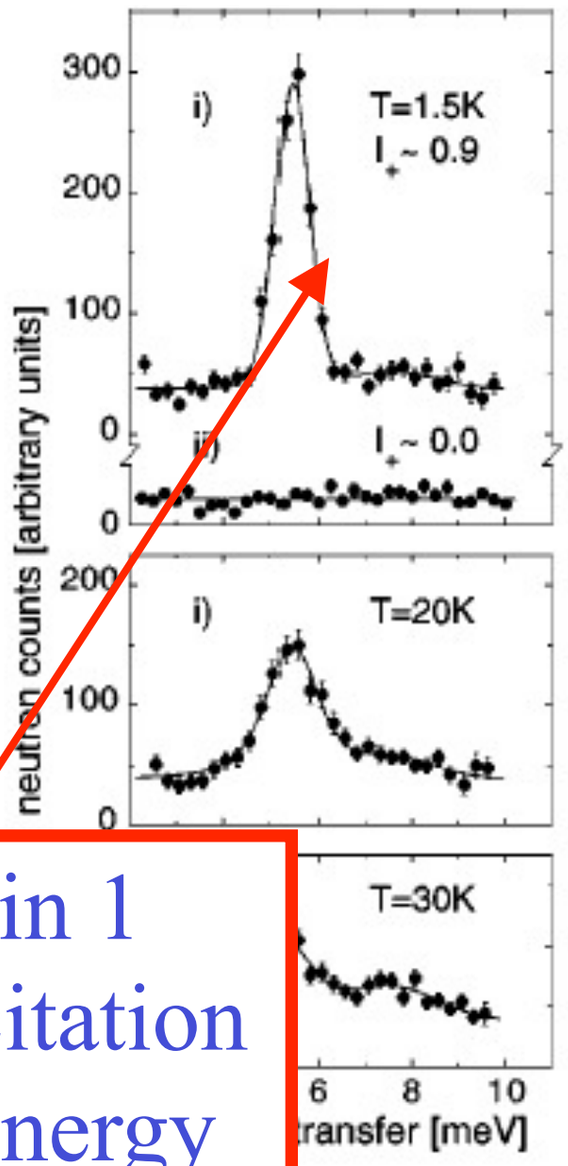

Sharp spin 1 particle excitation above an energy gap (spin gap)

les in the a^*c^* plane of $TlCuCl_3$ r.l.u]. The spectrum at $T = 1.5$ K

N. Cavadini, G. Heigold, W. Henggeler, A. Furrer, H.-U. Güdel, K. Krämer and H. Mutka, *Phys. Rev.* B 63 172414 (2001).

$TlCuCl_3$ with varying pressure

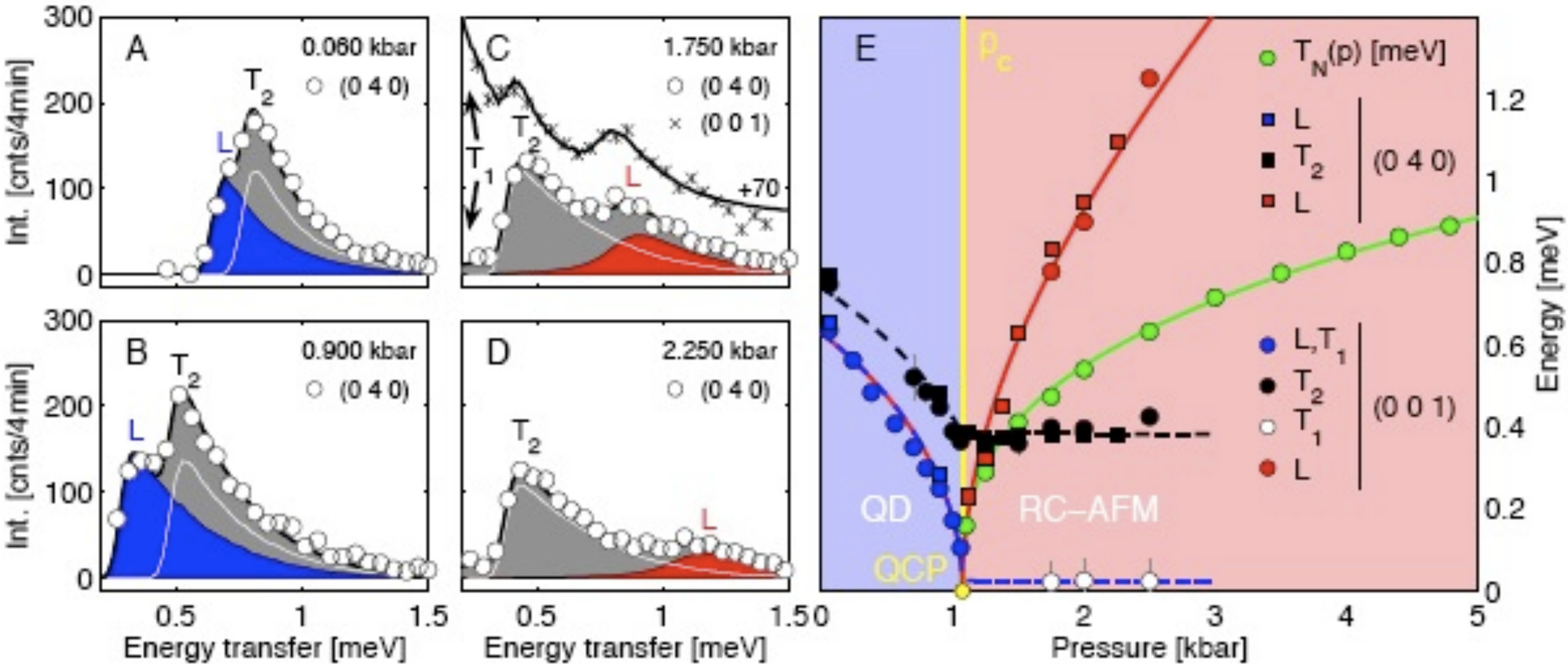

Observation of $3 \rightarrow 2$ low energy modes, emergence of new longitudinal mode (the "Higgs boson") in Néel phase, and vanishing of Néel temperature at quantum critical point

Christian Ruegg, Bruce Normand, Masashige Matsumoto, Albert Furrer, Desmond McMorrow, Karl Kramer, Hans–Ulrich Gudel, Severian Gvasaliya, Hannu Mutka, and Martin Boehm, *Phys. Rev. Lett.* **100**, 205701 (2008)

Prediction of quantum field theory

Potential for $\vec{\varphi}$ fluctuations: $V(\vec{\varphi}) = (\lambda - \lambda_c)\vec{\varphi}^2 + u\left(\vec{\varphi}^2\right)^2$

Paramagnetic phase, $\lambda > \lambda_c$

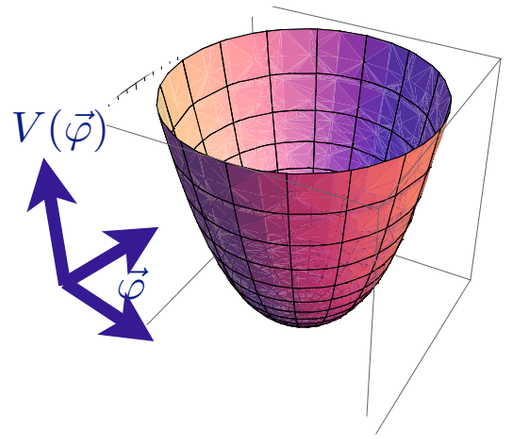

Expand about $\vec{\varphi} = 0$:

$$V(\vec{\varphi}) \approx (\lambda - \lambda_c)\vec{\varphi}^2$$

Yields 3 particles with energy gap $\sim \sqrt{(\lambda - \lambda_c)}$

Prediction of quantum field theory

Potential for $\vec{\varphi}$ fluctuations: $V(\vec{\varphi}) = (\lambda - \lambda_c)\vec{\varphi}^2 + u\left(\vec{\varphi}^2\right)^2$

Paramagnetic phase, $\lambda > \lambda_c$

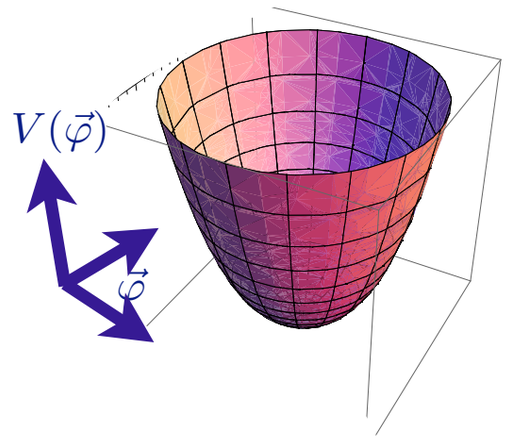

Expand about $\vec{\varphi} = 0$:

$$V(\vec{\varphi}) \approx (\lambda - \lambda_c)\vec{\varphi}^2$$

Yields 3 particles with energy gap $\sim \sqrt{(\lambda - \lambda_c)}$

Néel phase, $\lambda < \lambda_c$

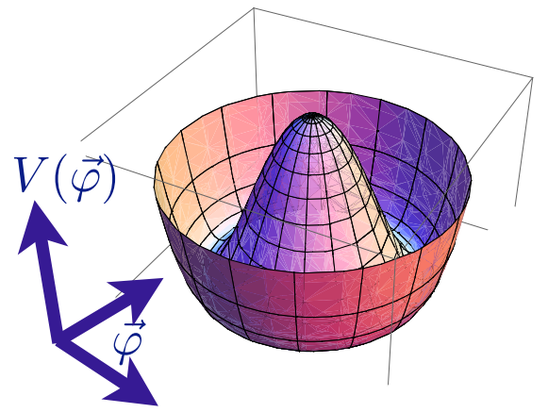

Expand $\vec{\varphi} = \left(0, 0, \sqrt{(\lambda_c - \lambda)/(2u)}\right) + \vec{\varphi}_1$:

$$V(\vec{\varphi}) \approx 2(\lambda_c - \lambda)\varphi_{1z}^2$$

Yields 2 gapless spin waves and one Higgs particle with energy gap $\sim \sqrt{2(\lambda_c - \lambda)}$

Prediction of quantum field theory

$$\frac{\text{Energy of Higgs particle}}{\text{Energy of triplon}} = \sqrt{2}$$

$$V(\vec{\varphi}) = (\lambda - \lambda_c)\vec{\varphi}^2 + u\left(\vec{\varphi}^2\right)^2$$

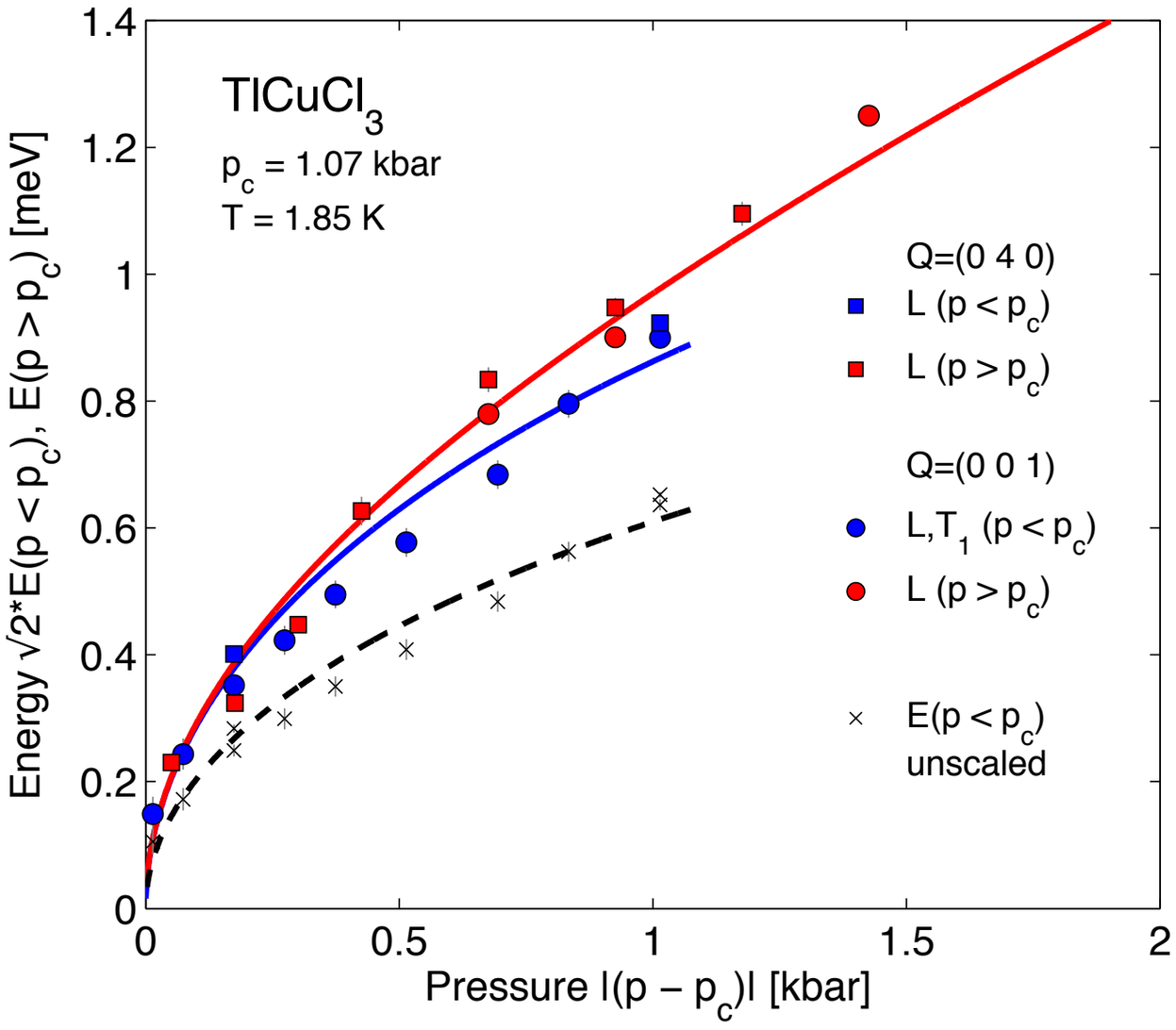

S. Sachdev, arXiv:0901.4103

Graphene

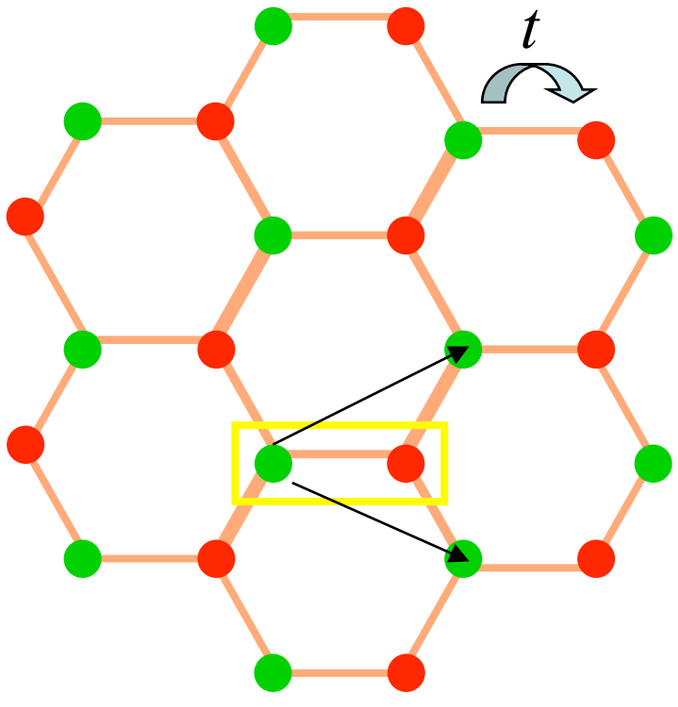

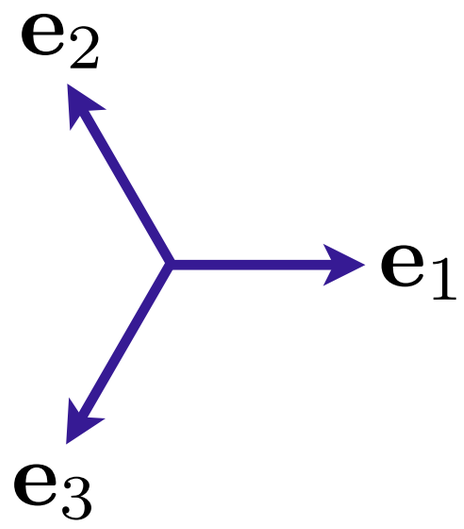

Graphene

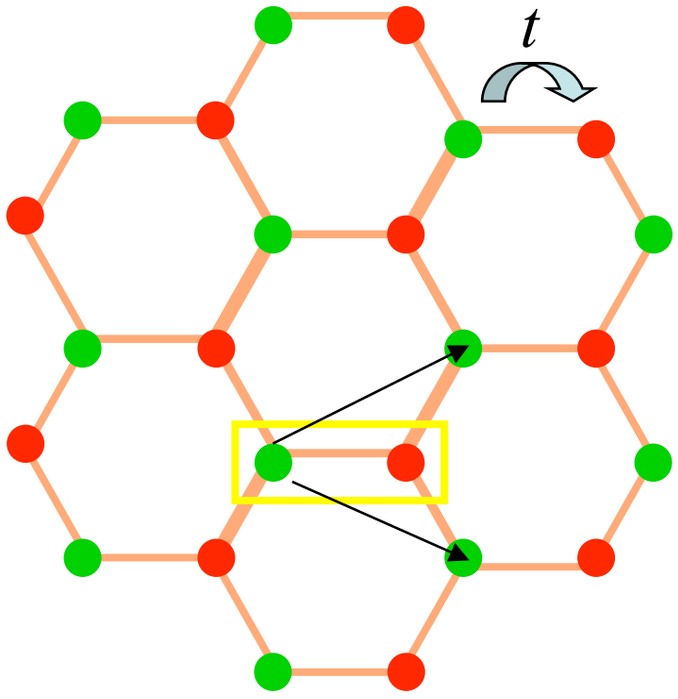

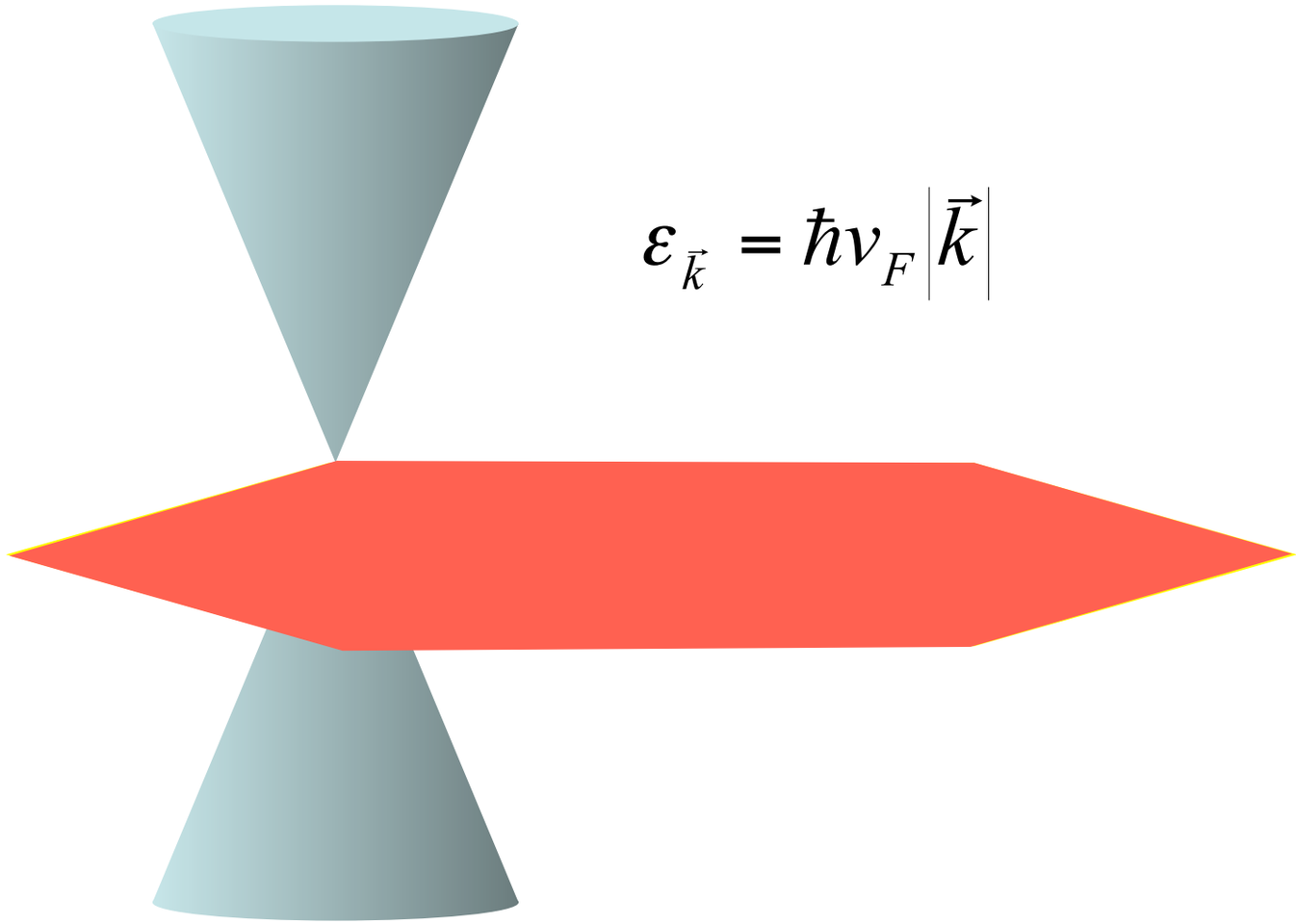

$$\varepsilon_{\vec{k}} = \hbar v_F \left| \vec{k} \right|$$

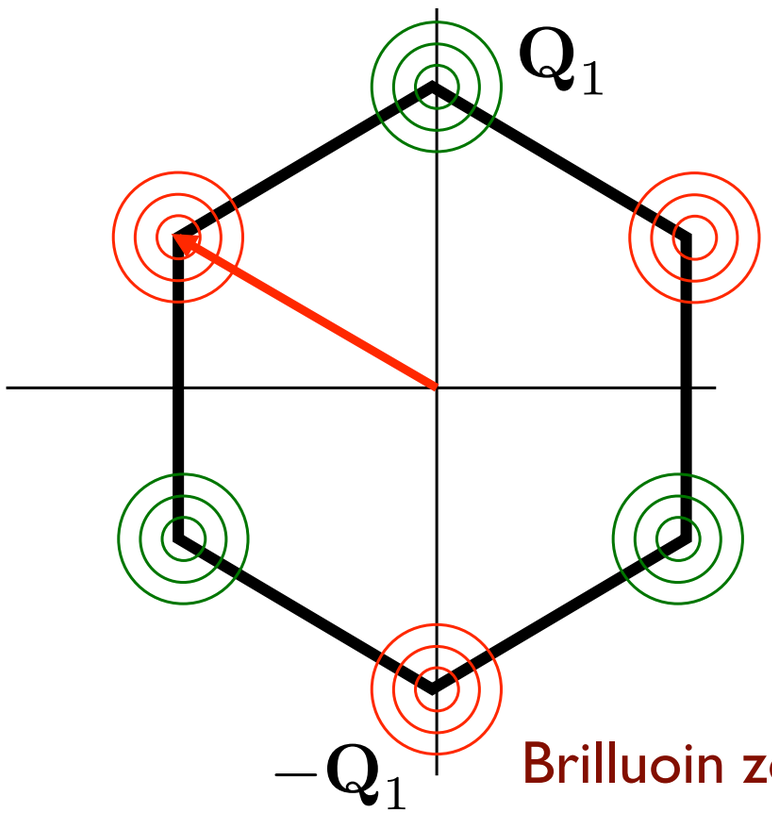

Brilluoin zone

Semi-metal with
massless Dirac fermions

Graphene

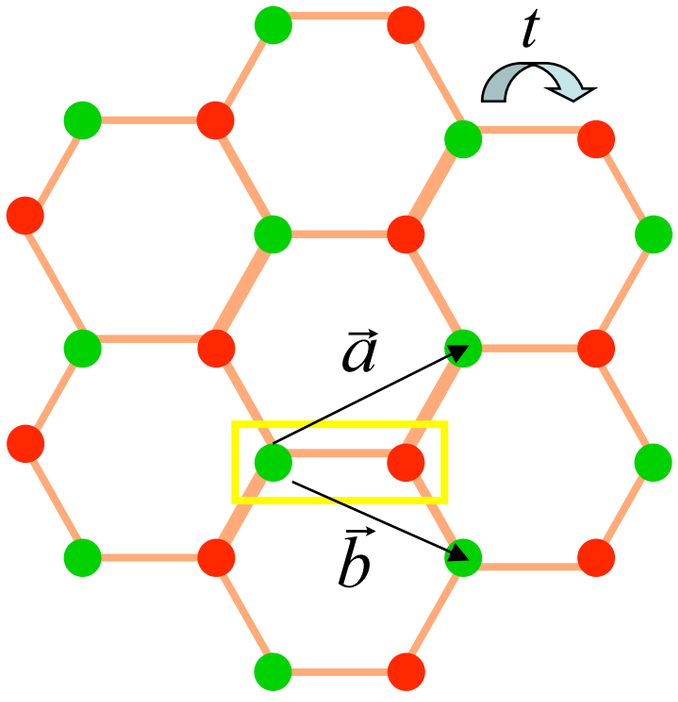

Dirac
semi-metal

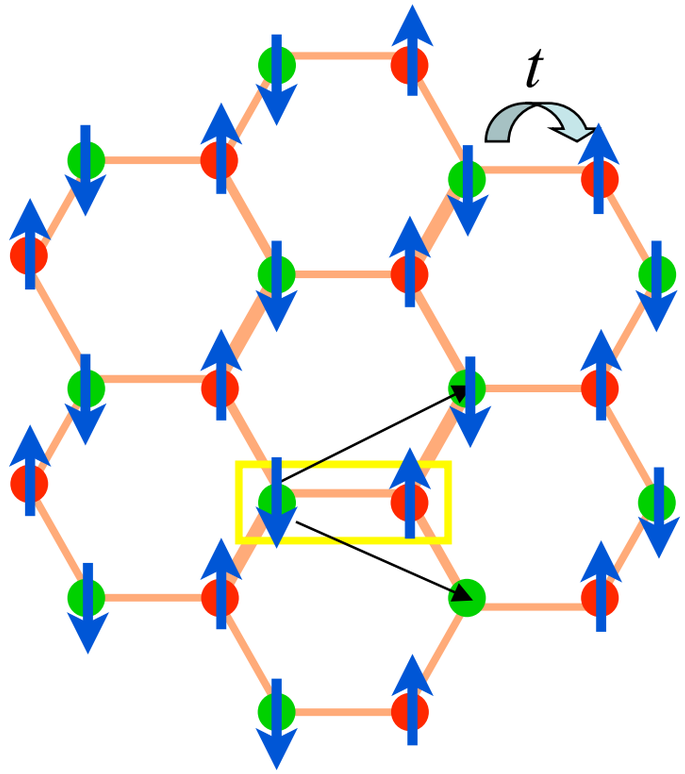

Insulating
antiferromagnet
with Neel order

U/t

I. HONEYCOMB LATTICE AT HALF FILLING

.

We define the unit length vectors

$$\mathbf{e}_1 = (1,0) \quad , \quad \mathbf{e}_2 = (-1/2, \sqrt{3}/2) \quad , \quad \mathbf{e}_3 = (-1/2, -\sqrt{3}/2). \tag{1}$$

Note that $\mathbf{e}_i \cdot \mathbf{e}_j = -1/2$ for $i \neq j$, and $\mathbf{e}_1 + \mathbf{e}_2 + \mathbf{e}_3 = 0$.

We take the origin of co-ordinates of the honeycomb lattice at the center of an *empty hexagon*. The A sublattice sites closest to the origin are at $\mathbf{e}_1$, $\mathbf{e}_2$, and $\mathbf{e}_3$, while the B sublattice sites closet to the origin are at $-\mathbf{e}_1$, $-\mathbf{e}_2$, and $-\mathbf{e}_3$.

The reciprocal lattice is generated by the wavevectors

$$\mathbf{G}_1 = \frac{4\pi}{3}\mathbf{e}_1 \quad , \quad \mathbf{G}_2 = \frac{4\pi}{3}\mathbf{e}_2 \quad , \quad \mathbf{G}_3 = \frac{4\pi}{3}\mathbf{e}_3 \tag{2}$$

The first Brillouin zone is a hexagon whose vertices are given by

$$\mathbf{Q}_1 = \frac{1}{3}(\mathbf{G}_2 - \mathbf{G}_3) \quad , \quad \mathbf{Q}_2 = \frac{1}{3}(\mathbf{G}_3 - \mathbf{G}_1) \quad , \quad \mathbf{Q}_3 = \frac{1}{3}(\mathbf{G}_1 - \mathbf{G}_2), \tag{3}$$

and $-\mathbf{Q}_1$, $-\mathbf{Q}_2$, and $-\mathbf{Q}_3$.

We define the Fourier transform of the fermions by

$$c_A(\mathbf{k}) = \sum_{\mathbf{r}} c_A(\mathbf{r}) e^{-i\mathbf{k}\cdot\mathbf{r}} \tag{4}$$

and similarly for c_B.

Now we define the continuum limit by the fields

$$\Psi_{A1} = c_A(\mathbf{Q}_1) \quad , \quad \Psi_{B1} = c_B(\mathbf{Q}_1) \quad , \quad \Psi_{A2} = c_A(-\mathbf{Q}_1) \quad , \quad \Psi_{B2} = c_B(-\mathbf{Q}_1) \tag{5}$$

The hopping Hamiltonian is

$$H_0 = -t \sum_{\langle ij \rangle} \left(c^\dagger_{Ai\alpha} c_{Bj\alpha} + c^\dagger_{Bj\alpha} c_{Ai\alpha} \right) \tag{6}$$

where α is a spin index. If we introduce Pauli matrices τ^a in sublattice space, this Hamiltonian can be written as

$$\begin{aligned} H_0 \; = \; \int \frac{d^2k}{4\pi^2} c^\dagger(\mathbf{k}) \Big[& -t \Big(\cos(\mathbf{k}\cdot\mathbf{e}_1) + \cos(\mathbf{k}\cdot\mathbf{e}_2) + \cos(\mathbf{k}\cdot\mathbf{e}_3) \Big) \tau^x \\ & + t \Big(\sin(\mathbf{k}\cdot\mathbf{e}_1) + \sin(\mathbf{k}\cdot\mathbf{e}_2) + \sin(\mathbf{k}\cdot\mathbf{e}_3) \Big) \tau^y \end{aligned} \tag{7}$$

The low energy excitations of this Hamiltonian are near $\mathbf{k} \approx \pm\mathbf{Q}_1$. In terms of the fields near $\mathbf{Q}_1$ and $-\mathbf{Q}_1$, we define

$$\begin{aligned}
\Psi_{A1\alpha}(\mathbf{k}) &= c_{A\alpha}(\mathbf{Q}+\mathbf{k}) \\
\Psi_{A2\alpha}(\mathbf{k}) &= c_{A\alpha}(-\mathbf{Q}+\mathbf{k}) \\
\Psi_{B1\alpha}(\mathbf{k}) &= c_{B\alpha}(\mathbf{Q}+\mathbf{k}) \\
\Psi_{B2\alpha}(\mathbf{k}) &= c_{B\alpha}(-\mathbf{Q}+\mathbf{k})
\end{aligned} \tag{8}$$

We consider Ψ to be a 8 component vector, and introduce Pauli matrices ρ^a which act in the $1,2$ valley space. Then the Hamiltonian is

$$H_0 = \int \frac{d^2k}{4\pi^2} \Psi^\dagger(\mathbf{k}) \Big(v\tau^y k_x + v\tau^x \rho^z k_y \Big) \Psi(\mathbf{k}), \tag{9}$$

where $v = 3t/2$; below we set $v = 1$. Now define $\overline{\Psi} = \Psi^\dagger \rho^z \tau^z$. Then we can write the imaginary time Lagrangian as

$$\mathcal{L}_0 = -i\overline{\Psi} \left(\omega\gamma_0 + k_x\gamma_1 + k_y\gamma_2 \right) \Psi \tag{10}$$

where

$$\gamma_0 = -\rho^z\tau^z \quad \gamma_1 = \rho^z\tau^x \quad \gamma_2 = -\tau^y \tag{11}$$

So the low energy theory has 4 2-component Dirac fermions.

A. Antiferromagnetism

We use the operator equation (valid on each site i):

$$U\left(n_\uparrow - \frac{1}{2}\right)\left(n_\downarrow - \frac{1}{2}\right) = -\frac{2U}{3} S^{a2} + \frac{U}{4} \tag{12}$$

Then we decouple the interaction via

$$\exp\left(\frac{2U}{3} \sum_i \int d\tau S_i^{a2} \right) = \int \mathcal{D}J_i^a(\tau) \exp\left(-\sum_i \int d\tau \left[\frac{3U}{8} J_i^{a2} - J_i^a S_i^a \right] \right) \tag{13}$$

We now integrate out the fermions, and look for the saddle point of the resulting effective action for J_i^a. At the saddle-point we find that the lowest energy is achieved when the vector has opposite orientations on the A and B sublattices. Anticipating this, we look for a continuum limit in terms of a field φ^a where

$$J_A^a = \varphi^a \quad , \quad J_B^a = -\varphi^a \tag{14}$$

The coupling between the field φ^a and the Ψ fermions is given by

$$\sum_i J_i^a c_{i\alpha}^\dagger \sigma_{\alpha\beta}^a c_{i\beta} = \varphi^a \left(c_{A\alpha}^\dagger \sigma_{\alpha\beta}^a c_{A\beta} - c_{B\alpha}^\dagger \sigma_{\alpha\beta}^a c_{B\beta} \right) = \varphi^a \Psi^\dagger \tau^z \sigma^a \Psi = -\varphi^a \overline{\Psi} \rho^z \sigma^a \Psi \tag{15}$$

From this we motivate the low energy theory

$$\mathcal{L} = \overline{\Psi} \gamma_\mu \partial_\mu \Psi + \frac{1}{2} \left[\left(\partial_\mu \varphi^a \right)^2 + \varphi^{a2} \right] + \frac{u}{24} \left(\varphi^{a2} \right)^2 - \lambda \varphi^a \overline{\Psi} \rho^z \sigma^a \Psi \tag{16}$$

Note that the matrix $\rho^z \sigma^a$ commutes with all the γ_μ; hence $\rho^z \sigma^a$ is a matrix in "flavor" space. This is the Gross-Neveu model, and it describes the quantum phase transition from the Dirac semi-metal to an insulating Néel state. In the Néel state, we have $\varphi^a = N_0 \delta_{az}$ (say), and so the dispersion of the electrons is

$$\omega_k = \pm \sqrt{k^2 + \lambda^2 N_0^2} \tag{17}$$

near the points $\pm \mathbf{Q}_1$. These form the conduction and valence bands of the insulator.